US005961745A

United States Patent [19]

Inoue et al.

[11] **Patent Number: 5,961,745**

[45] **Date of Patent: Oct. 5, 1999**

[54] **FE BASED SOFT MAGNETIC GLASSY ALLOY**

[75] Inventors: **Akihisa Inoue**, 11-806 Kawauchijutaku, 35banchi, Motohasekura, Aoba-ku, Sendai-shi, Miyagi-ken; **Takao Mizushima**, Niigata-ken; **Kouichi Fujita**, Miyagi-ken; **Oki Yamaguchi**; **Akihiro Makino**, both of Niigata-ken, all of Japan

[73] Assignees: **Alps Electric Co., Ltd.**; **Akihisa Inoue**; **Japan Science and Technology Corp.**, all of, Japan

[21] Appl. No.: **08/832,325**

[22] Filed: **Mar. 26, 1997**

[30] **Foreign Application Priority Data**

Mar. 25, 1996 [JP] Japan 8-068818
Sep. 13, 1996 [JP] Japan 8-243756

[51] **Int. Cl.**[6] **H01F 1/153**

[52] **U.S. Cl.** **148/304**; 148/403

[58] **Field of Search** 148/304, 403

[56] **References Cited**

U.S. PATENT DOCUMENTS

4,859,256	8/1989	Sawa et al.	148/304
5,032,196	7/1991	Masumoto et al.	148/403
5,312,495	5/1994	Masumoto et al.	148/550
5,362,339	11/1994	Horimura et al.	148/403
5,738,733	4/1998	Inoue	148/403

Primary Examiner—John Sheehan
Attorney, Agent, or Firm—Brinks Hofer Gilson & Lione

[57] **ABSTRACT**

The present invention is directed to provide a Fe based glassy alloy which exhibits soft magnetic characteristics at room temperature, has a thickness greater than that of a conventional amorphous alloy prepared by a liquid quenching process and can be easily formed in bulk. The Fe based glassy alloy in accordance with the present invention has a temperature distance ΔT_x, expressed by the equation $\Delta T_x = T_x - T_g$, of a supercooled liquid of not less than 35° C., wherein Tx indicates crystallization temperature and Tg represents glass transition temperature.

1 Claim, 27 Drawing Sheets

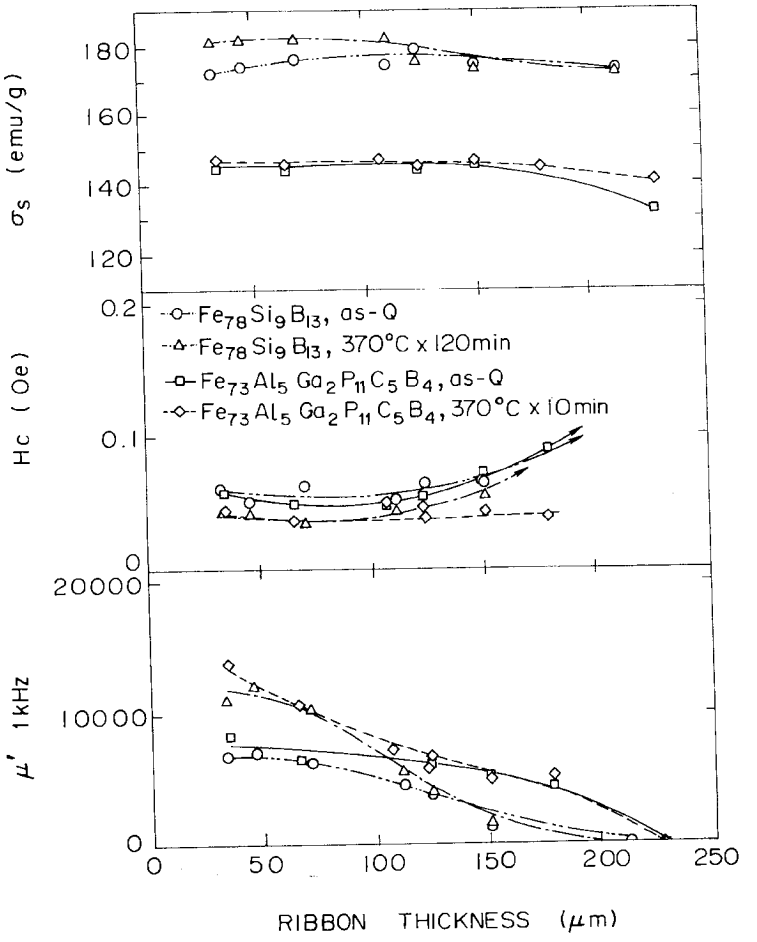

FIG. 1

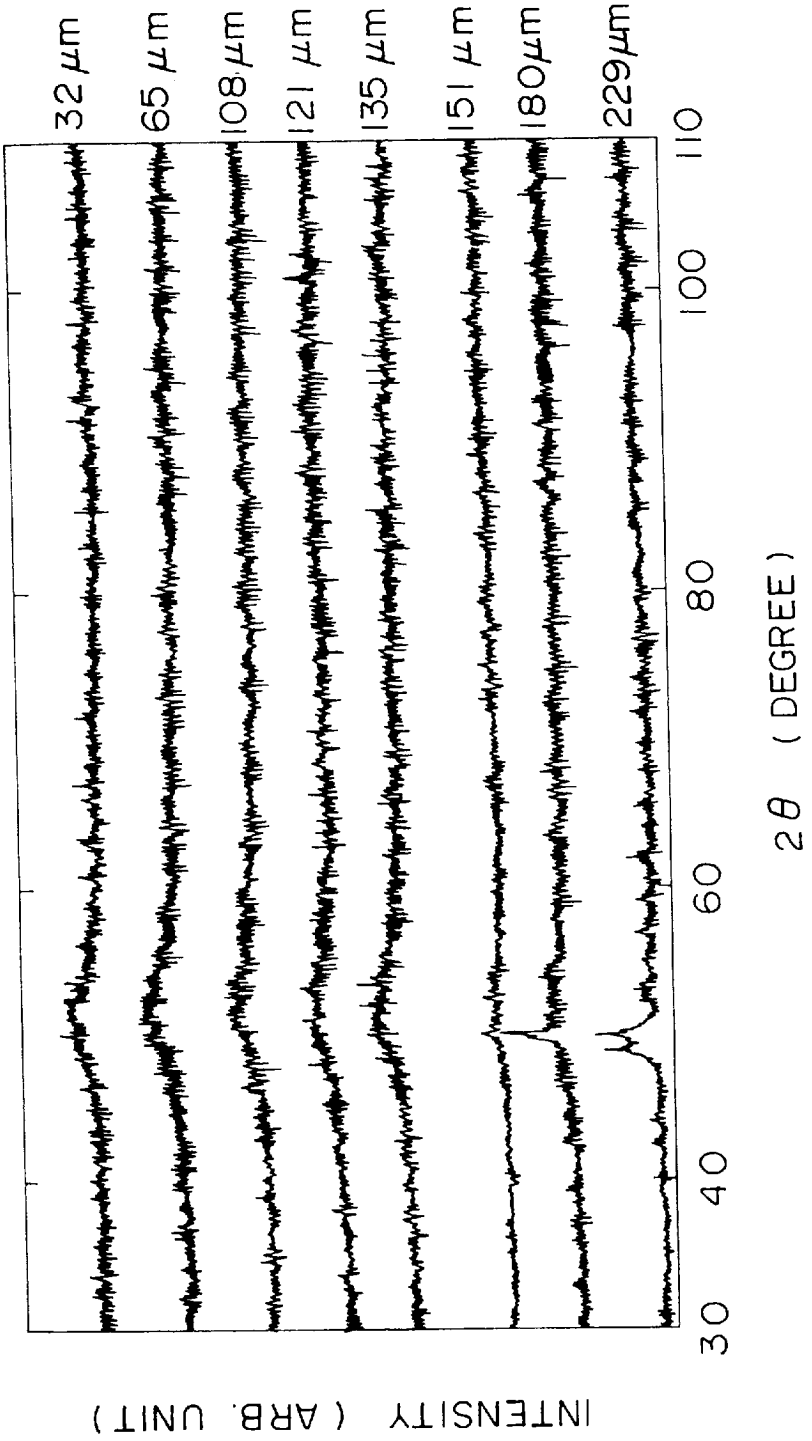
32 μm
65 μm
108 μm
121 μm
135 μm
151 μm
180μm
229μm
30
40
60
80
100
110
2θ (DEGREE)
INTENSITY (ARB. UNIT)

FIG. 2

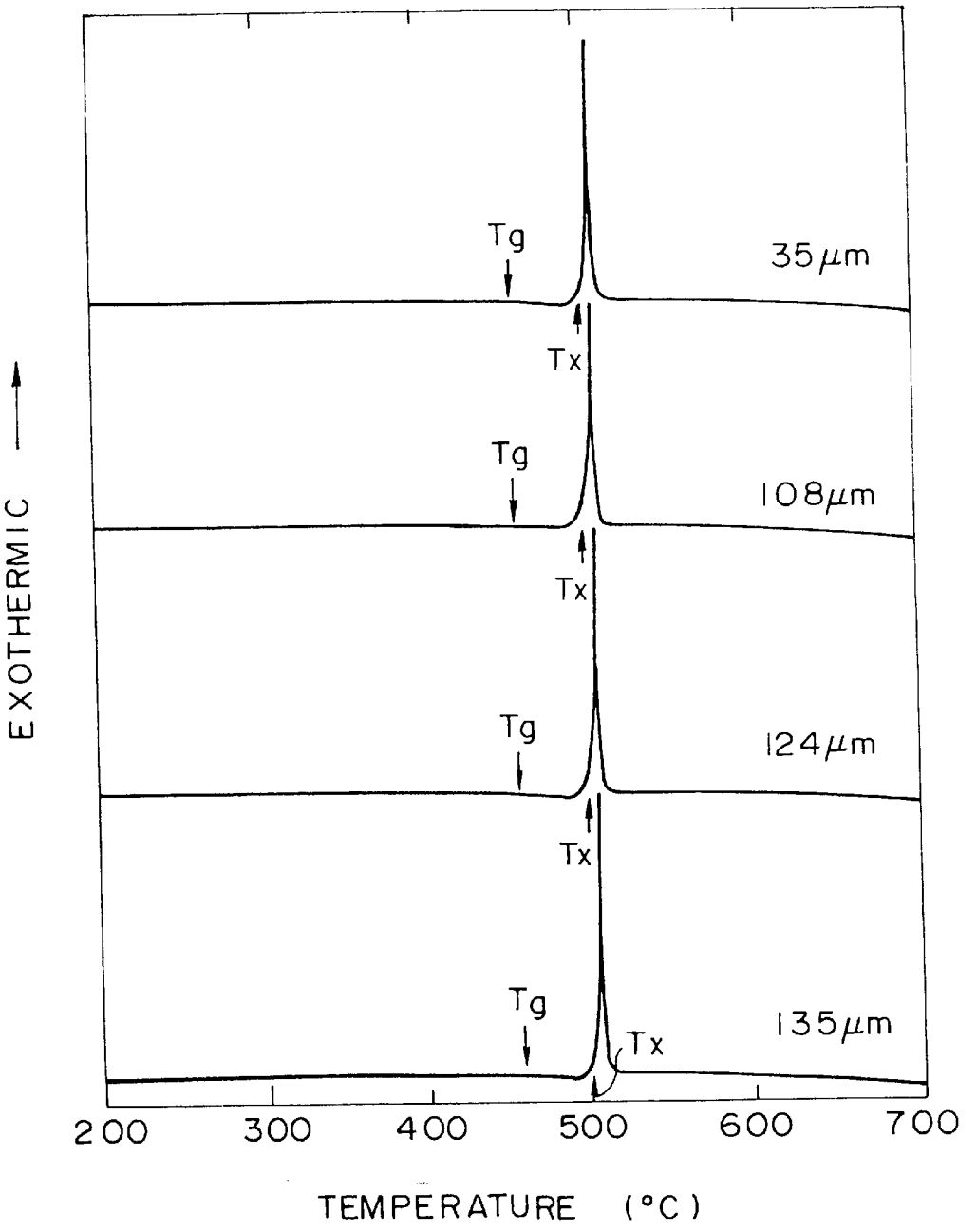
Tg
35μm
Tx
Tg
108μm
Tx
Tg
124μm
Tx
Tg
135μm
Tx
EXOTHERMIC
200
300
400
500
600
700
TEMPERATURE (°C)

FIG. 3

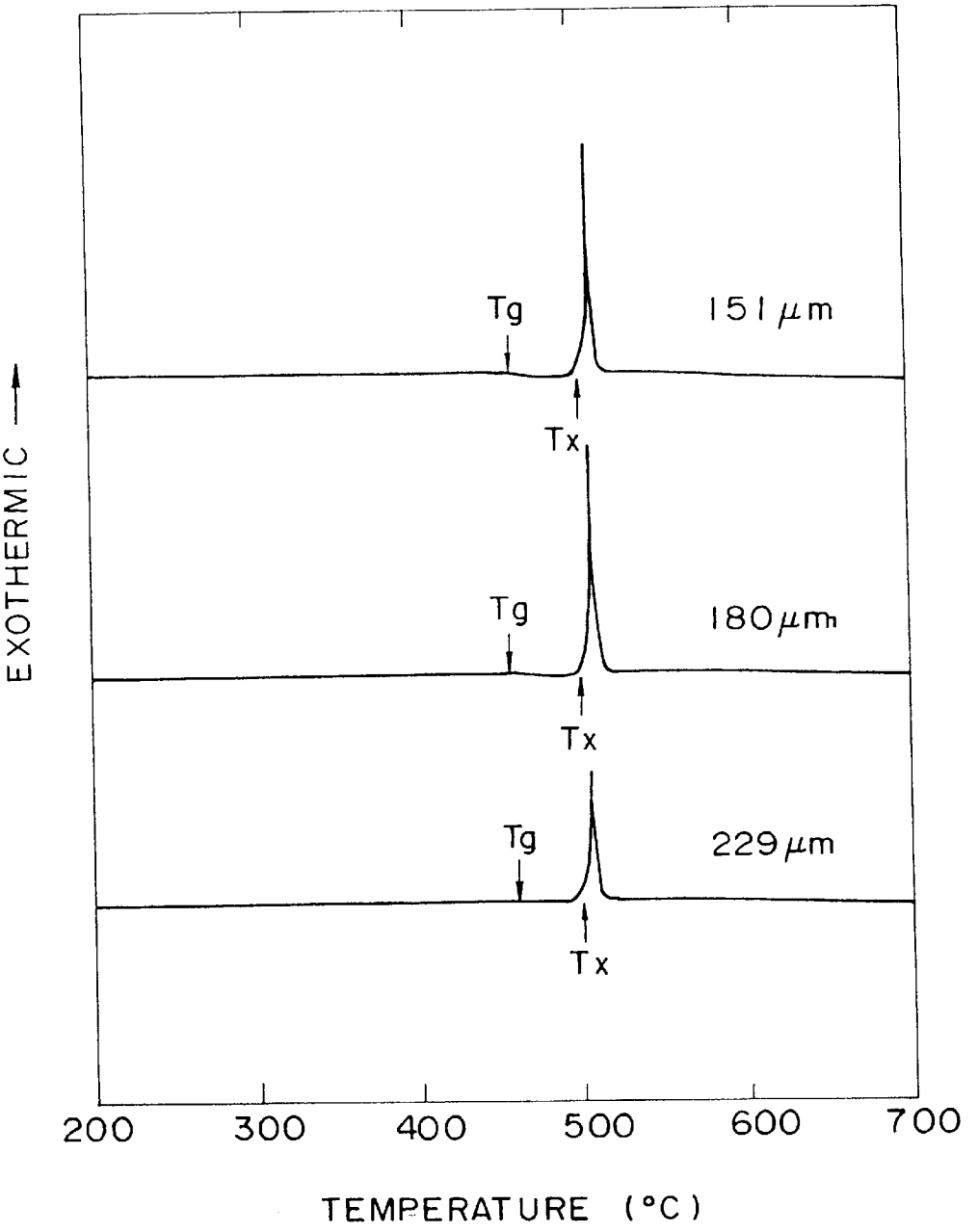
EXOTHERMIC
Tg
Tx
151 μm
Tg
Tx
180 μm
Tg
Tx
229 μm
200
300
400
500
600
700
TEMPERATURE (°C)

FIG. 4

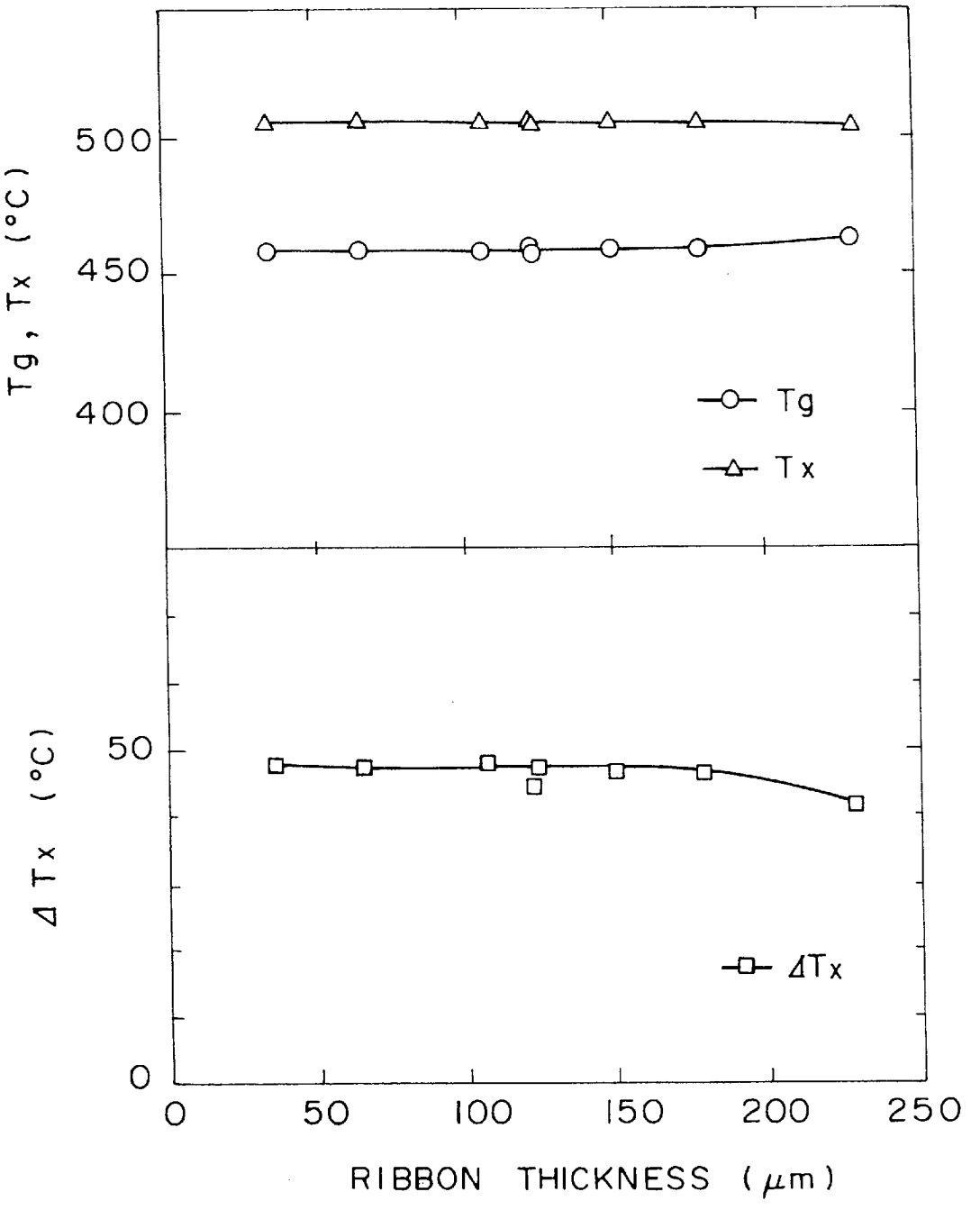
500
450
400
Tg , Tx (°C)
Tg
Tx
50
0
ΔTx (°C)
ΔTx
0
50
100
150
200
250
RIBBON THICKNESS (μm)

FIG. 5

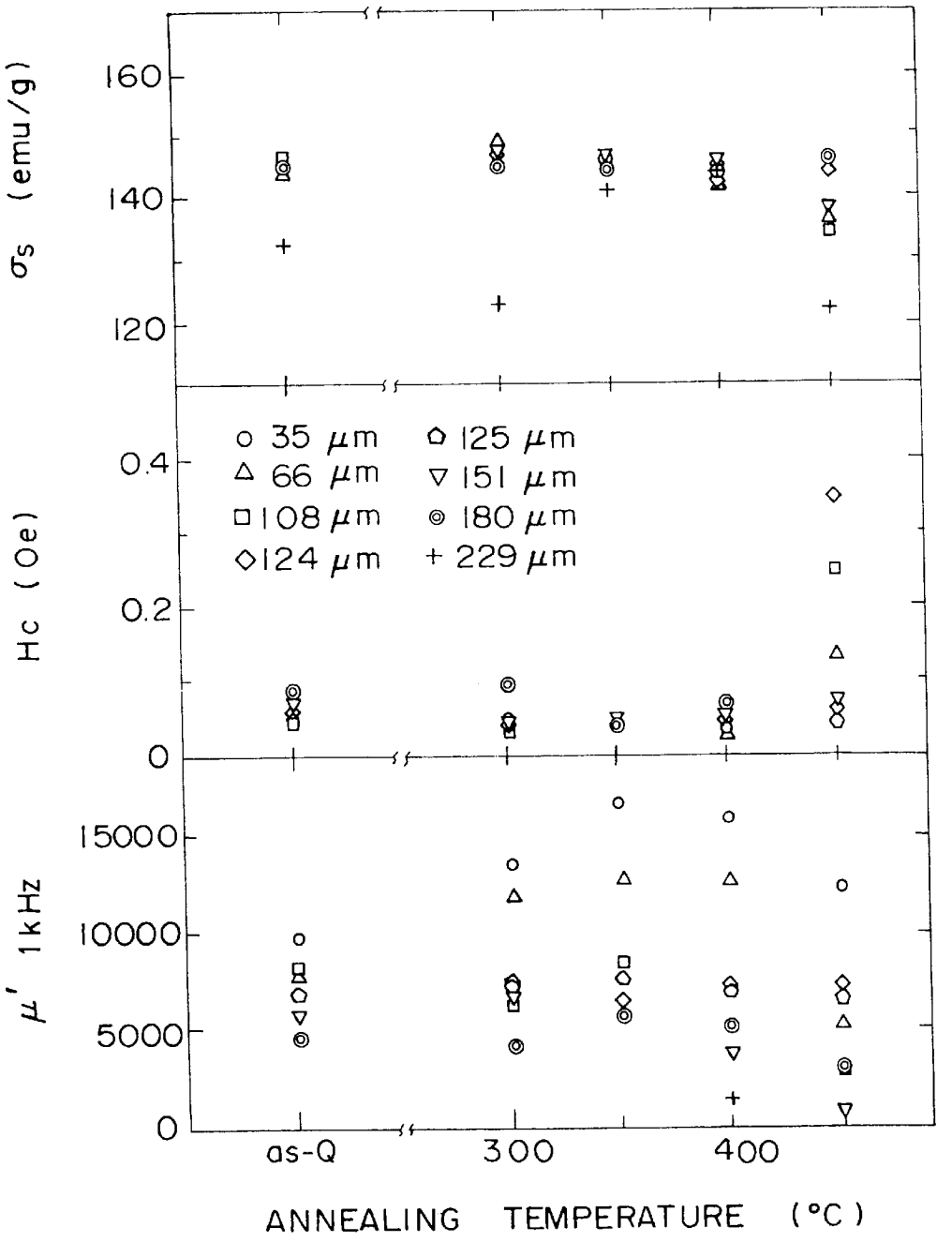
σs (emu/g)
160
140
120
Hc (Oe)
0.4
0.2
0
μ' 1kHz
15000
10000
5000
0
○ 35 μm
△ 66 μm
□ 108 μm
◇ 124 μm
⬠ 125 μm
▽ 151 μm
◎ 180 μm
+ 229 μm
as-Q
300
400
ANNEALING TEMPERATURE (°C)

FIG. 6

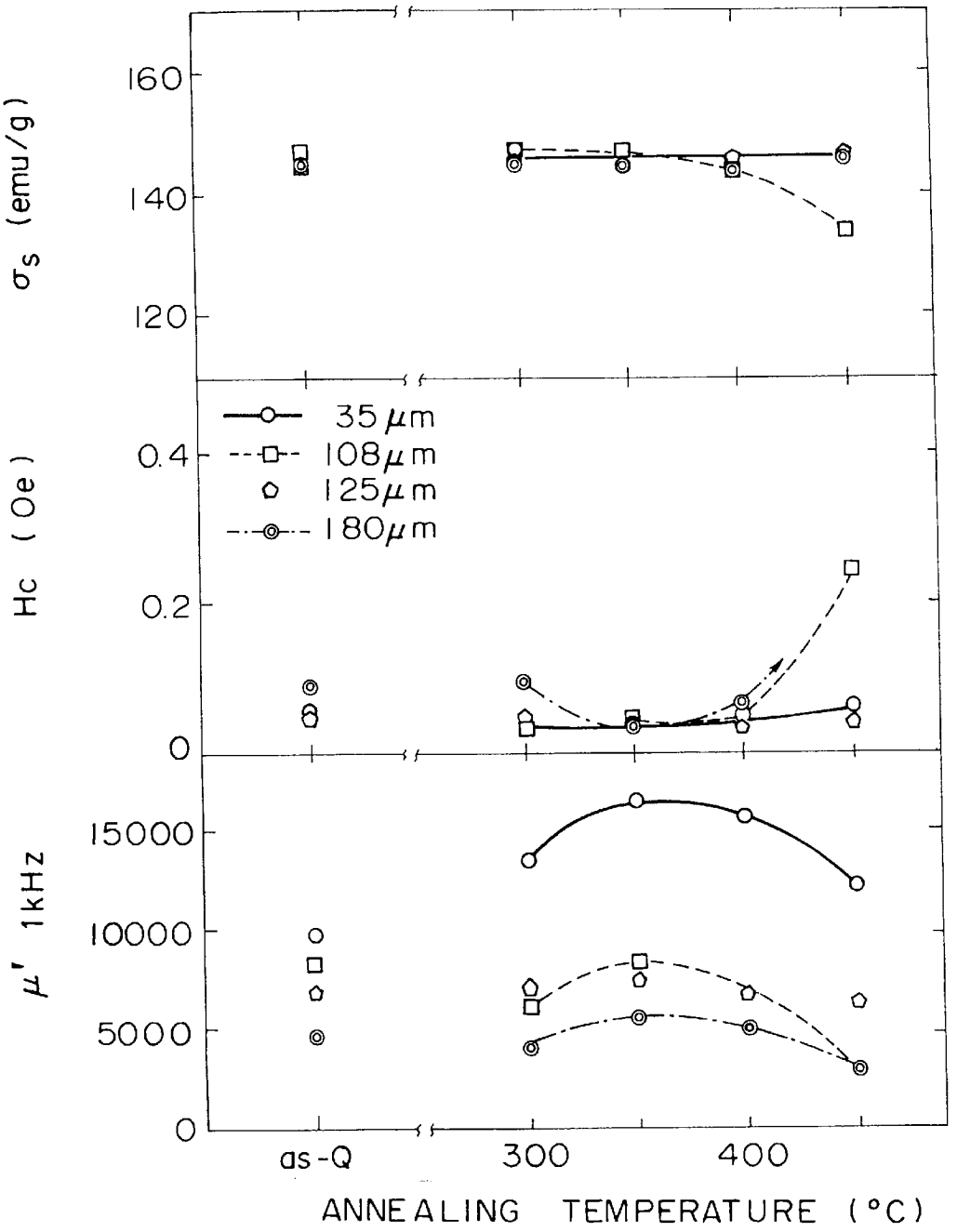
160
140
120
σs (emu/g)
35 μm
108 μm
125 μm
180 μm
0.4
0.2
0
Hc (Oe)
15000
10000
5000
0
μ' 1kHz
as-Q
300
400
ANNEALING TEMPERATURE (°C)

FIG. 7

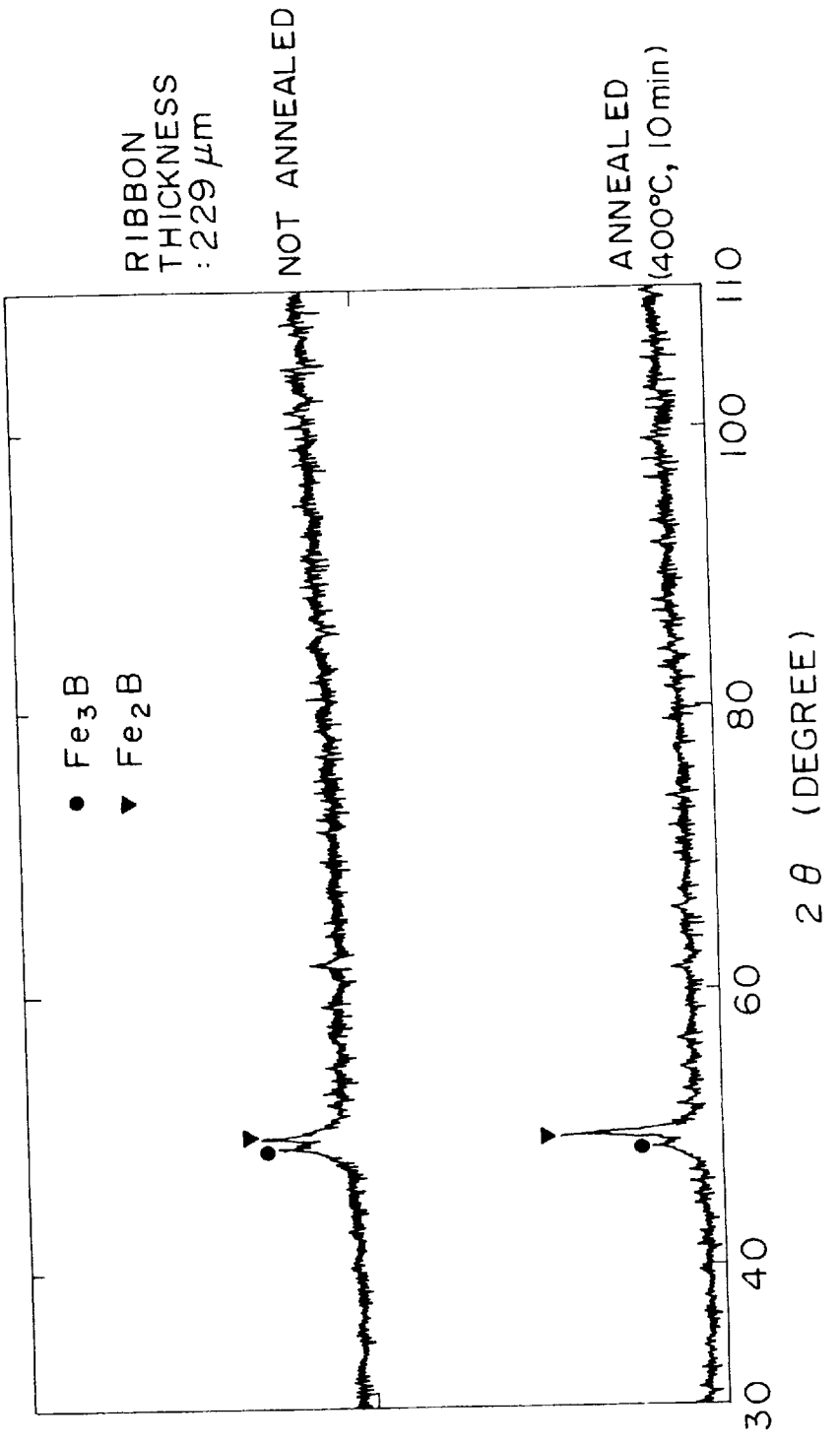
RIBBON THICKNESS : 229 μm
NOT ANNEALED
ANNEALED (400°C, 10 min)
● Fe3B
▼ Fe2B
30
40
60
80
100
110
2θ (DEGREE)

FIG. 8

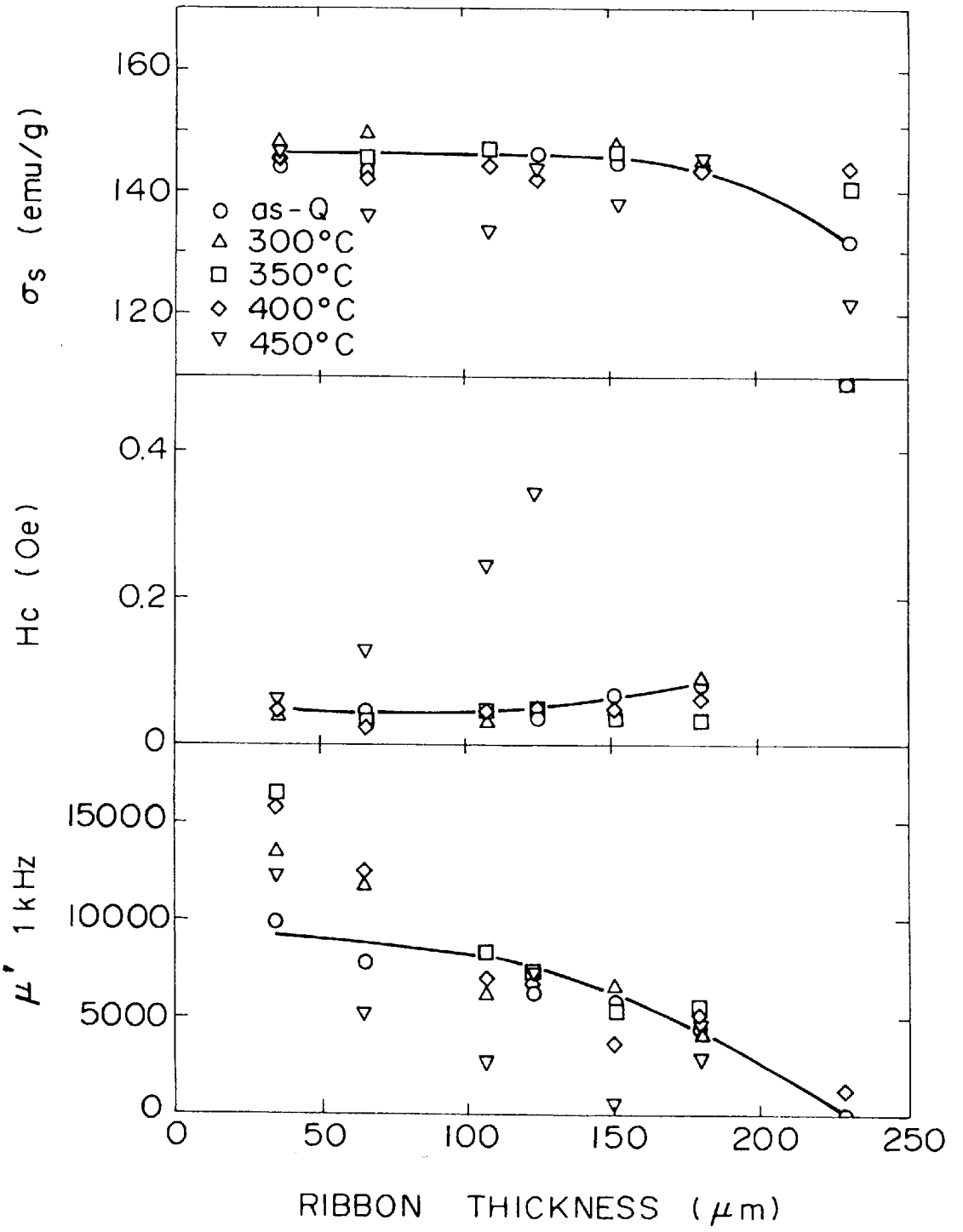
160
140
120
σs (emu/g)
as-Q
300°C
350°C
400°C
450°C
0.4
0.2
0
Hc (Oe)
15000
10000
5000
0
μ' 1kHz
0
50
100
150
200
250
RIBBON THICKNESS (μm)

FIG. 9

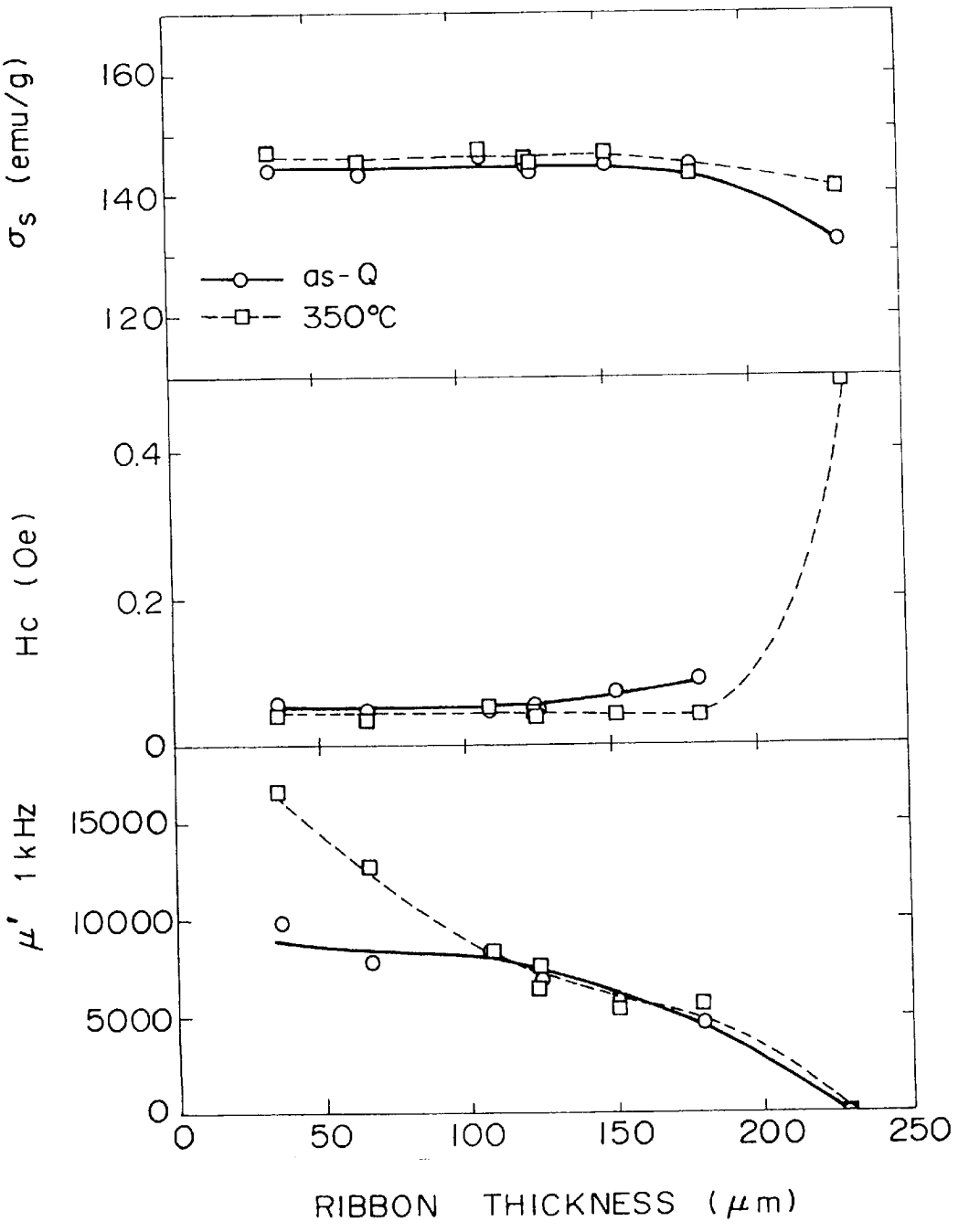
σs (emu/g)
160
140
120
as-Q
350°C
Hc (Oe)
0.4
0.2
0
μ' 1 kHz
15000
10000
5000
0
0
50
100
150
200
250
RIBBON THICKNESS (μm)

FIG. 10

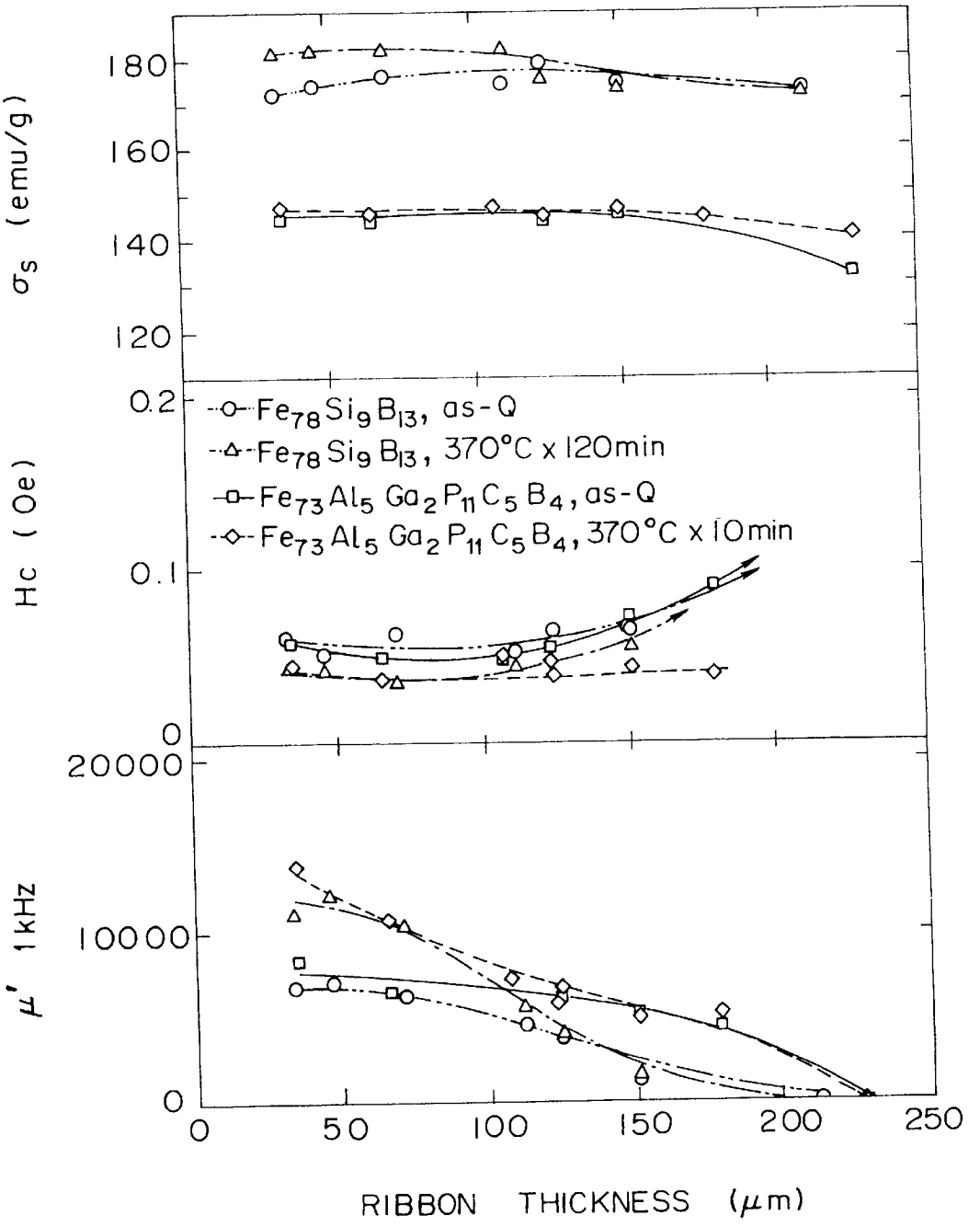
180
160
140
120
σ_s (emu/g)
0.2
0.1
0
Hc (Oe)
$Fe_{78}Si_9B_{13}$, as-Q
$Fe_{78}Si_9B_{13}$, 370°C x 120min
$Fe_{73}Al_5Ga_2P_{11}C_5B_4$, as-Q
$Fe_{73}Al_5Ga_2P_{11}C_5B_4$, 370°C x 10min
20000
10000
0
μ' 1kHz
0
50
100
150
200
250
RIBBON THICKNESS (μm)

FIG. 11

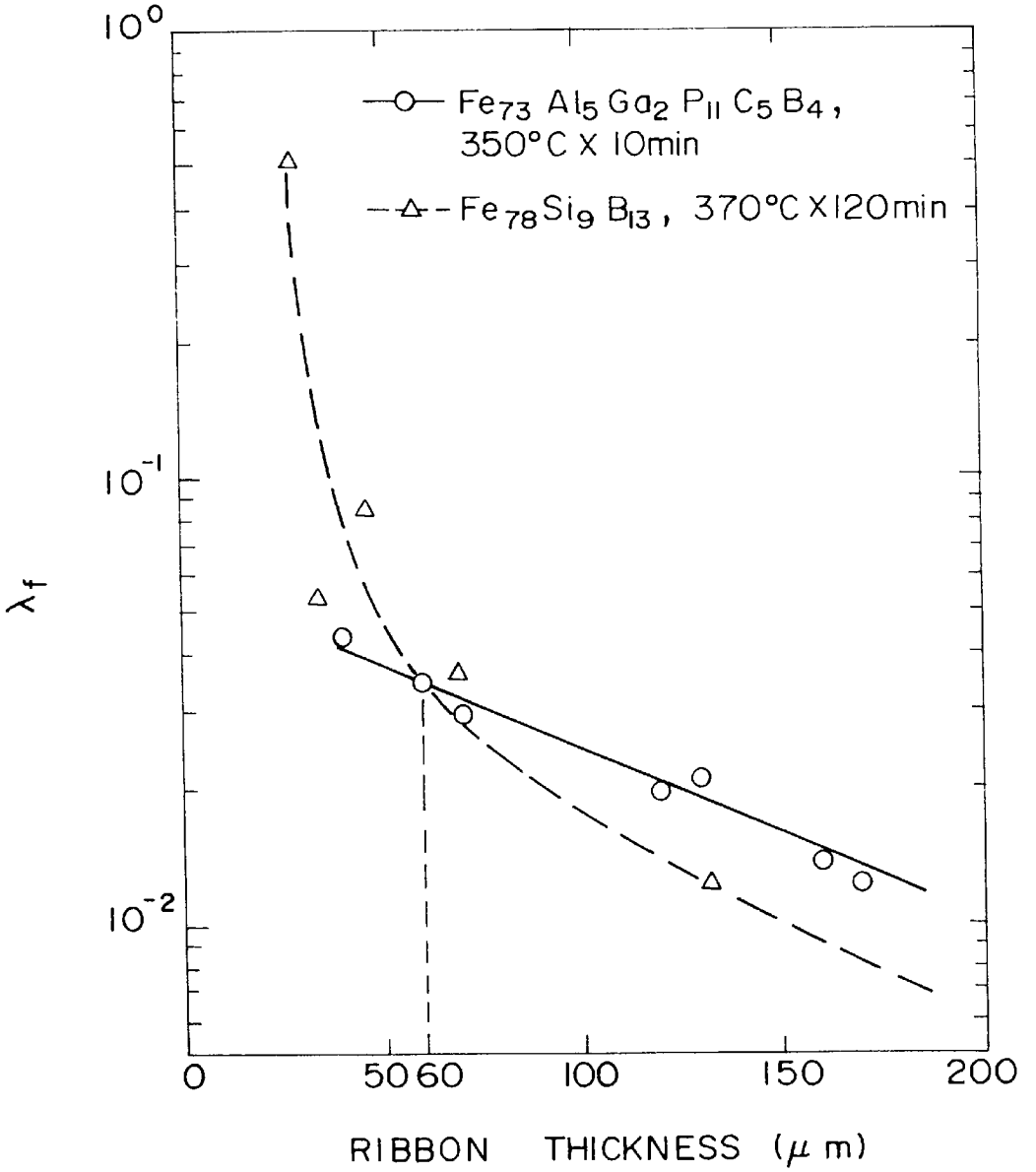
10^0
10^{-1}
10^{-2}
λ_f
$Fe_{73}Al_5Ga_2P_{11}C_5B_4$, 350°C X 10min
$Fe_{78}Si_9B_{13}$, 370°C X120min
0
50 60
100
150
200
RIBBON THICKNESS (μm)

FIG. 12

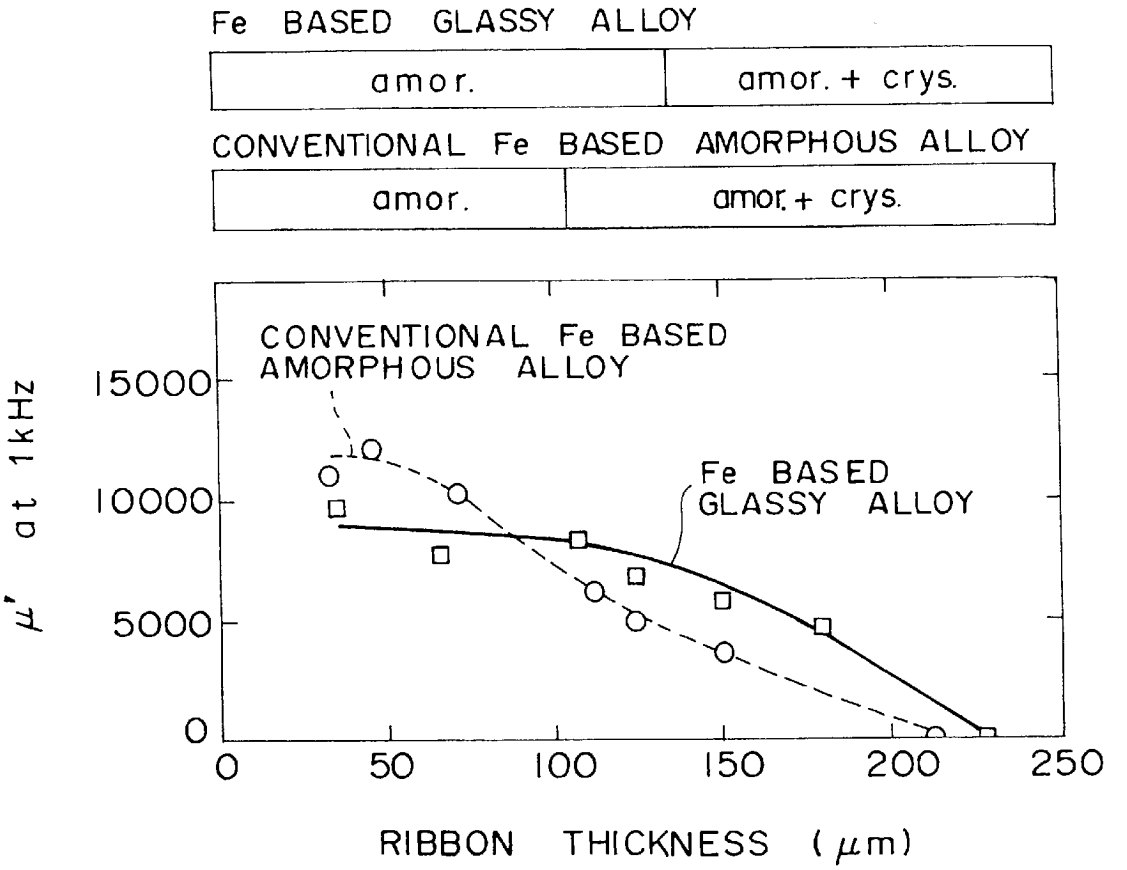
Fe BASED GLASSY ALLOY
amor.
amor. + crys.
CONVENTIONAL Fe BASED AMORPHOUS ALLOY
amor.
amor. + crys.
CONVENTIONAL Fe BASED AMORPHOUS ALLOY
Fe BASED GLASSY ALLOY
μ' at 1kHz
15000
10000
5000
0
0
50
100
150
200
250
RIBBON THICKNESS (μm)

FIG. 13

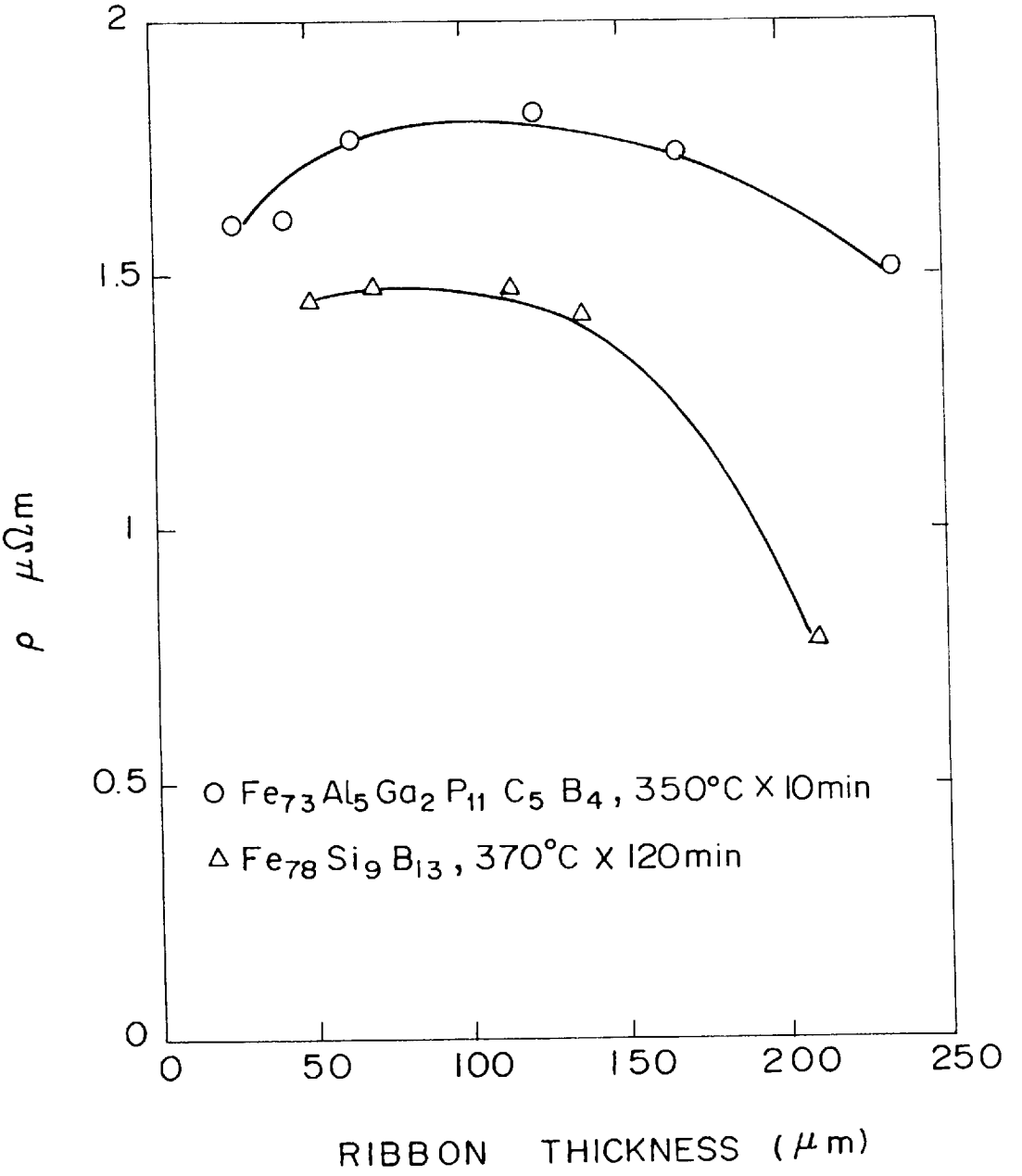
2
1.5
1
0.5
0
ρ μΩm
0
50
100
150
200
250
RIBBON THICKNESS (μm)
○ Fe73 Al5 Ga2 P11 C5 B4 , 350°C X 10min
△ Fe78 Si9 B13 , 370°C X 120min

FIG. 14

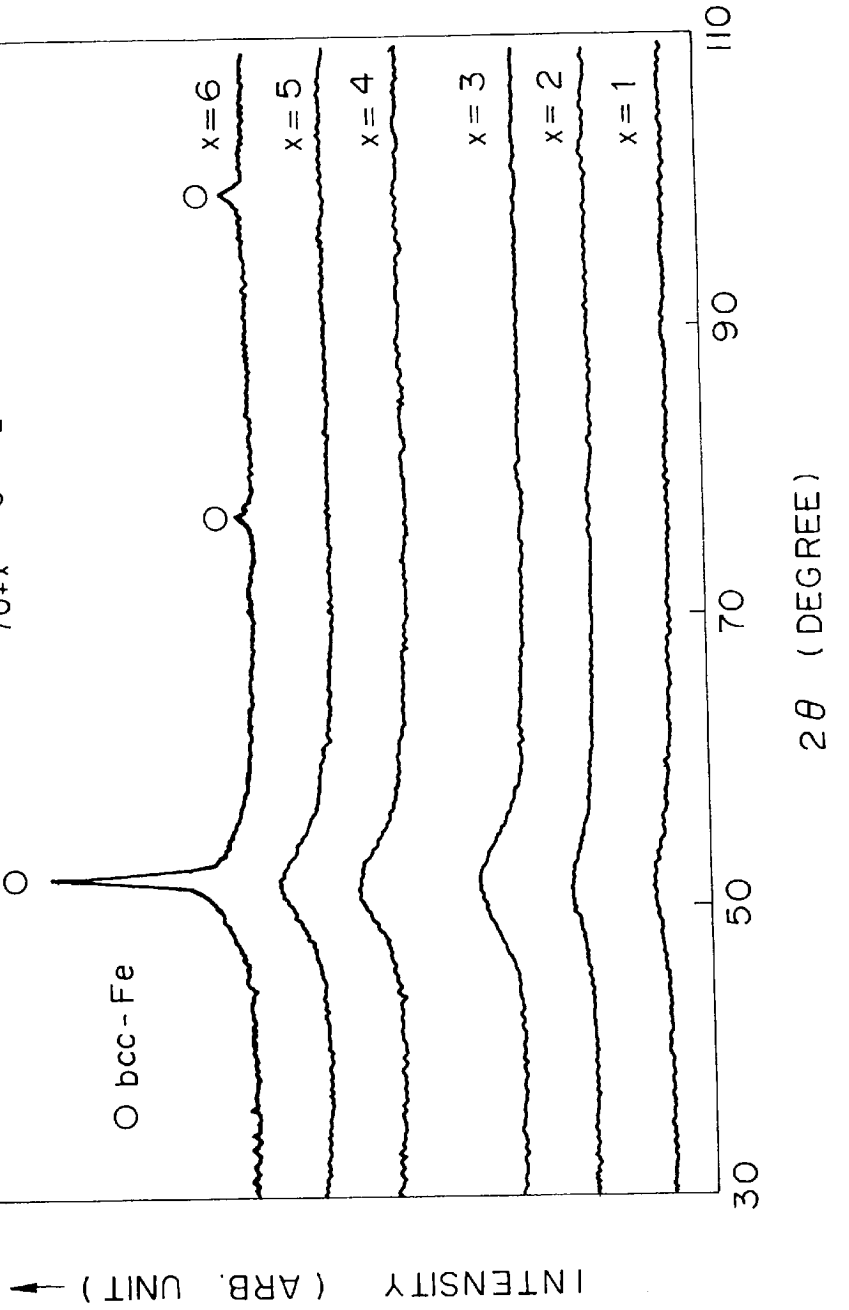
$Fe_{70+x}Al_5Ga_2(P_{55}C_{25}B_{20})_{23-x}$
O bcc-Fe
O
O
O x=6
x=5
x=4
x=3
x=2
x=1
30
50
70
90
110
2θ (DEGREE)
INTENSITY (ARB. UNIT)

FIG. 15

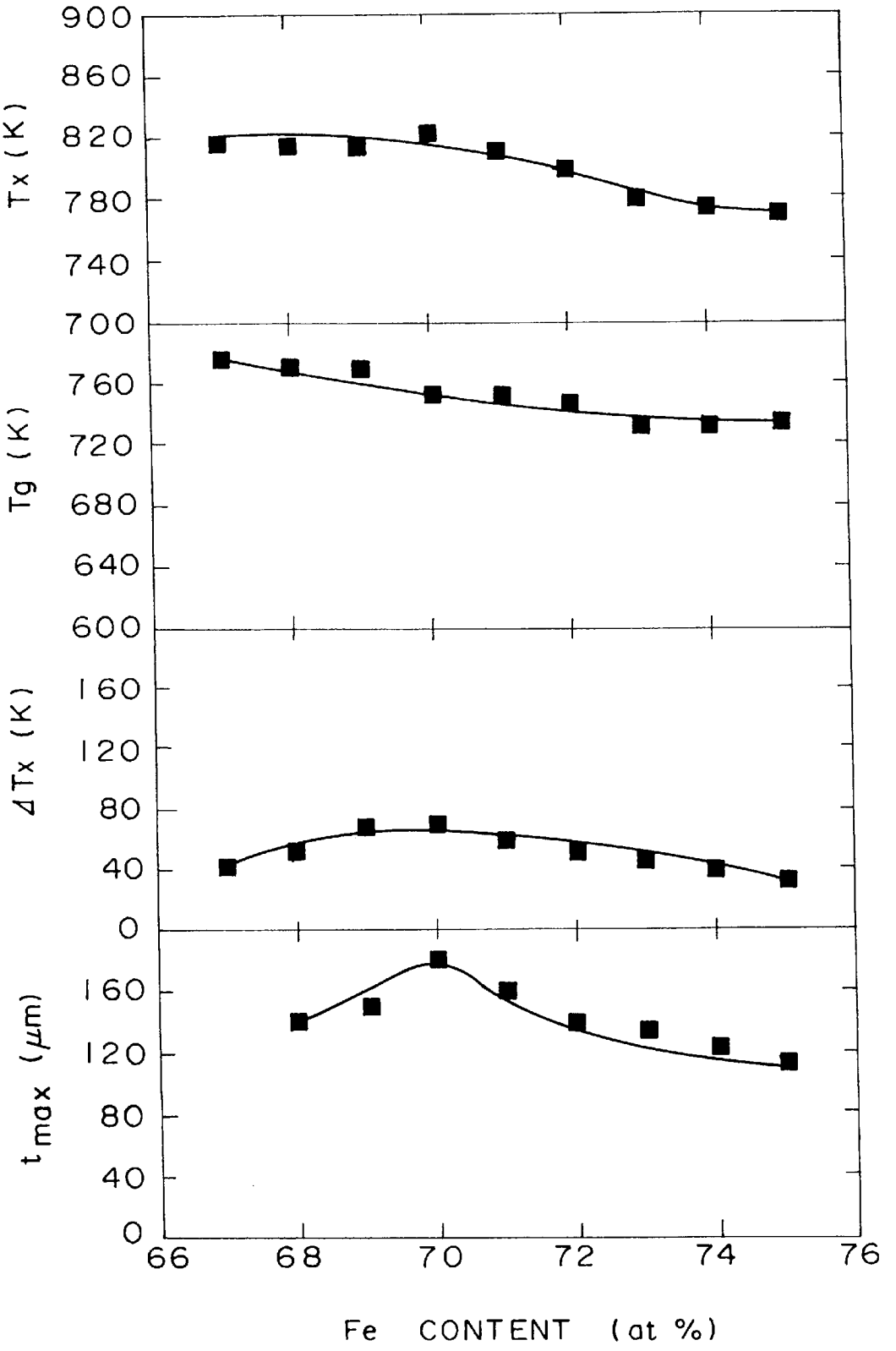
Tx (K)
900
860
820
780
740
700
Tg (K)
760
720
680
640
600
ΔTx (K)
160
120
80
40
0
t max (μm)
160
120
80
40
0
66
68
70
72
74
76
Fe CONTENT (at %)

FIG. 16

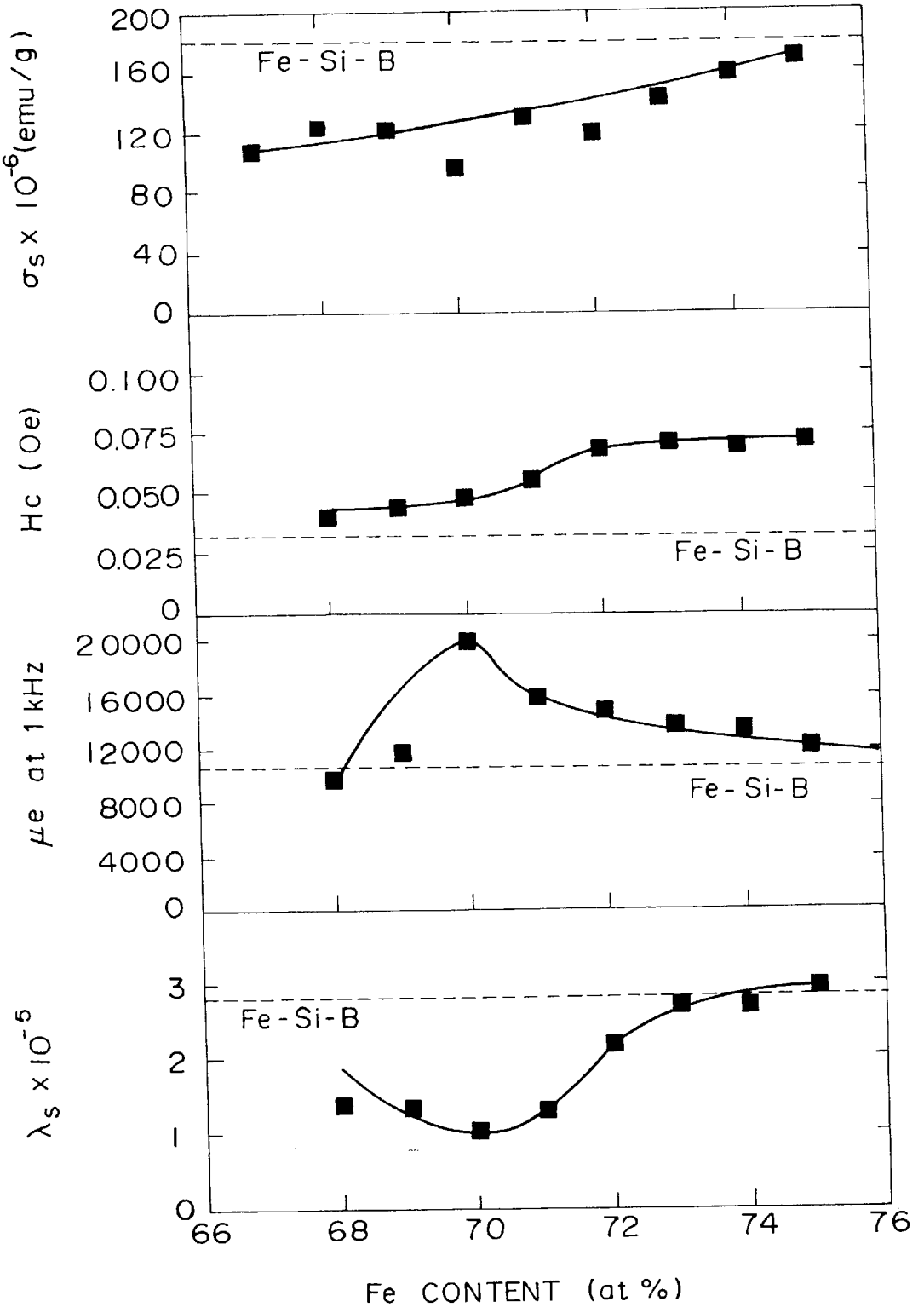
Fe-Si-B
$\sigma_s \times 10^{-6}$(emu/g)
200
160
120
80
40
0
Hc (Oe)
0.100
0.075
0.050
0.025
0
Fe-Si-B
μe at 1 kHz
20000
16000
12000
8000
4000
0
Fe-Si-B
$\lambda_s \times 10^{-5}$
3
2
1
0
Fe-Si-B
66
68
70
72
74
76
Fe CONTENT (at %)

FIG. 17

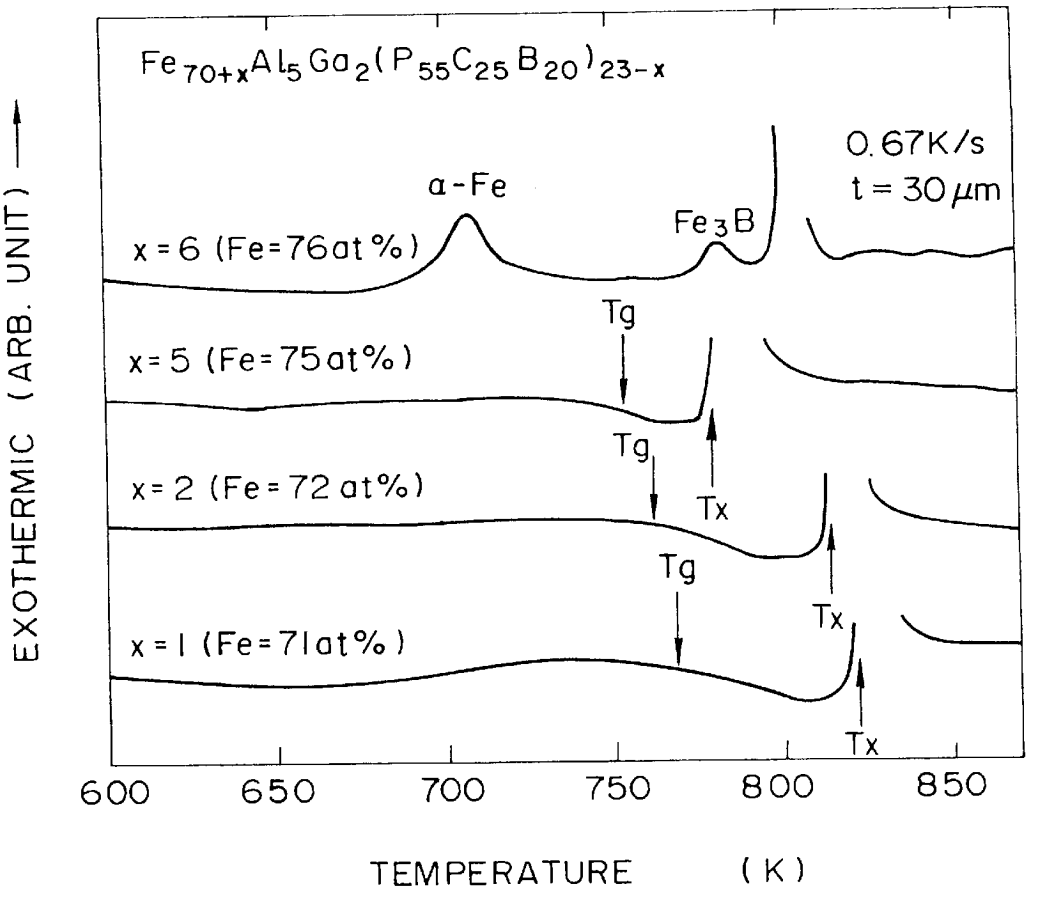
$Fe_{70+x}Al_5Ga_2(P_{55}C_{25}B_{20})_{23-x}$
0.67K/s
t = 30 μm
α-Fe
Fe_3B
x = 6 (Fe=76at%)
Tg
x = 5 (Fe=75at%)
Tg
Tx
x = 2 (Fe=72at%)
Tg
Tx
x = 1 (Fe=71at%)
Tx
EXOTHERMIC (ARB. UNIT)
600
650
700
750
800
850
TEMPERATURE (K)

FIG. 18

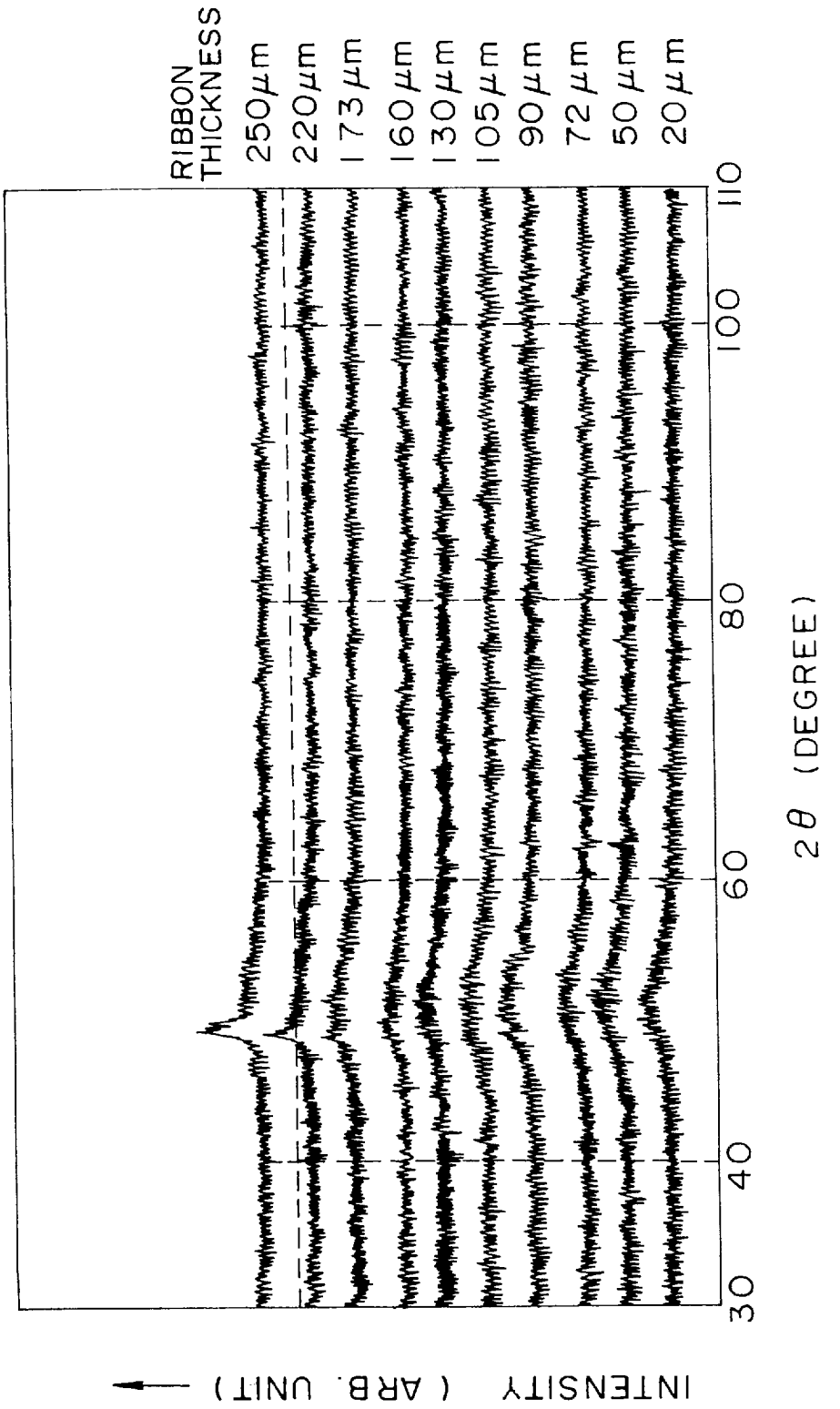
RIBBON THICKNESS
250μm
220μm
173μm
160μm
130μm
105μm
90μm
72μm
50μm
20μm
30
40
60
80
100
110
2θ (DEGREE)
INTENSITY (ARB. UNIT)

FIG. 19

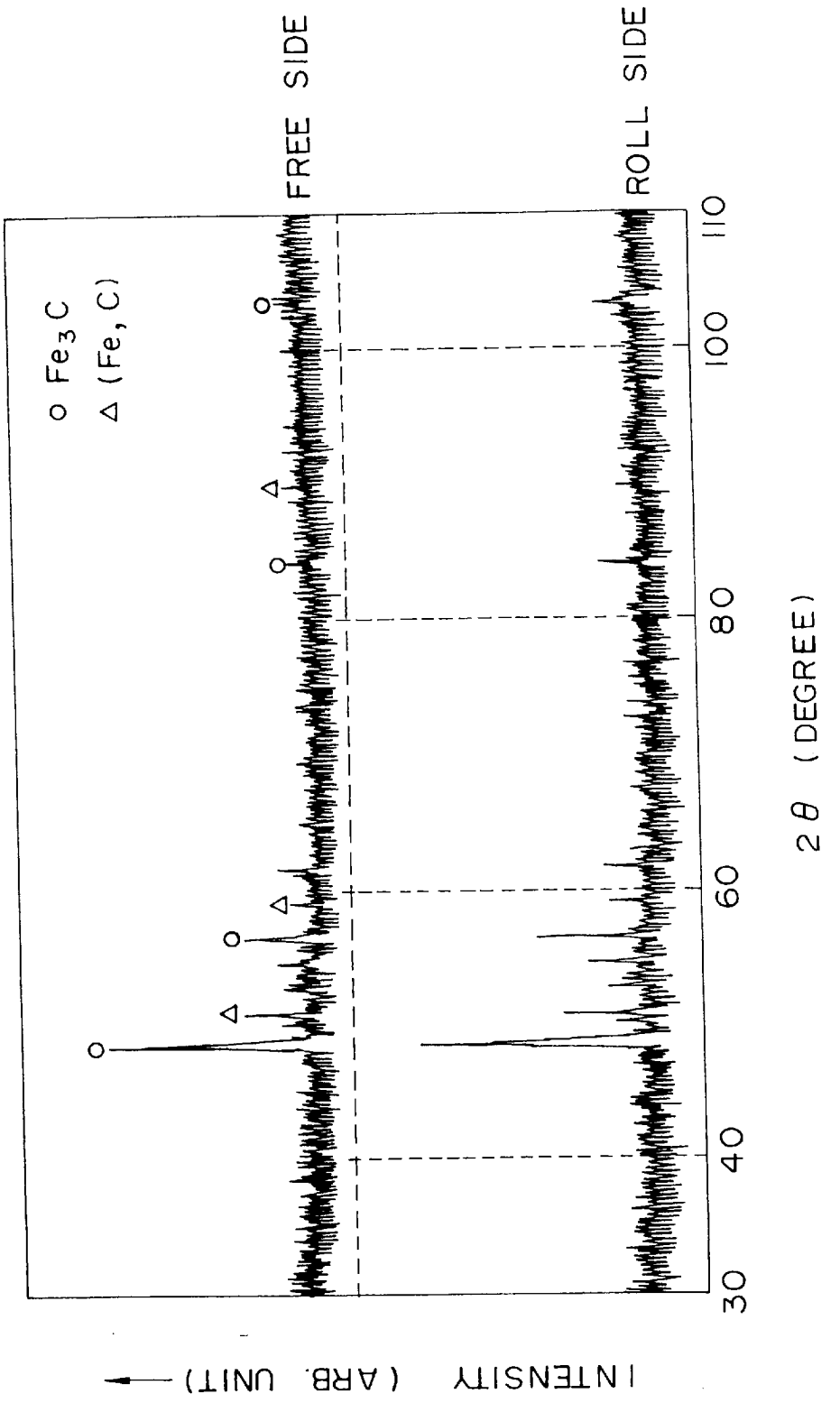
FREE SIDE
ROLL SIDE
o Fe_3C
Δ (Fe, C)
INTENSITY (ARB. UNIT)
2θ (DEGREE)
30
40
60
80
100
110

FIG. 20

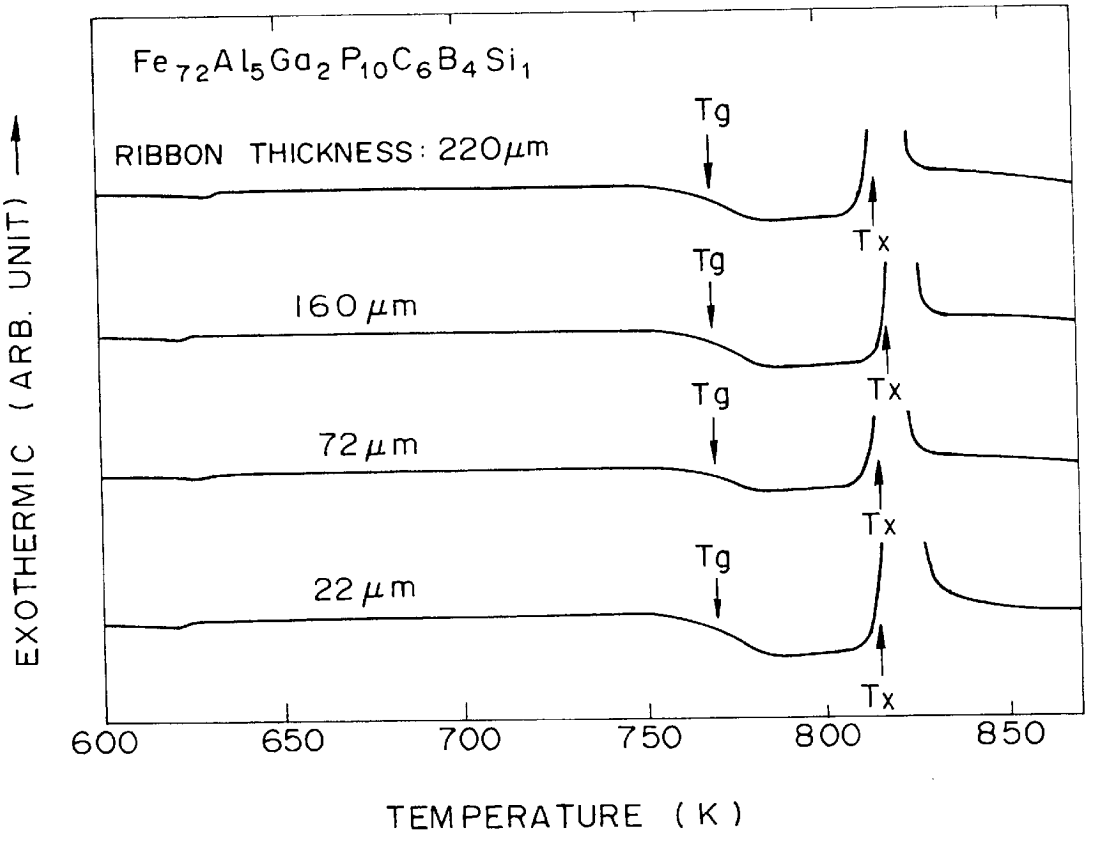
$Fe_{72}Al_5Ga_2P_{10}C_6B_4Si_1$
RIBBON THICKNESS: 220μm
160 μm
72 μm
22 μm
Tg
Tx
EXOTHERMIC (ARB. UNIT)
600
650
700
750
800
850
TEMPERATURE (K)

FIG. 21

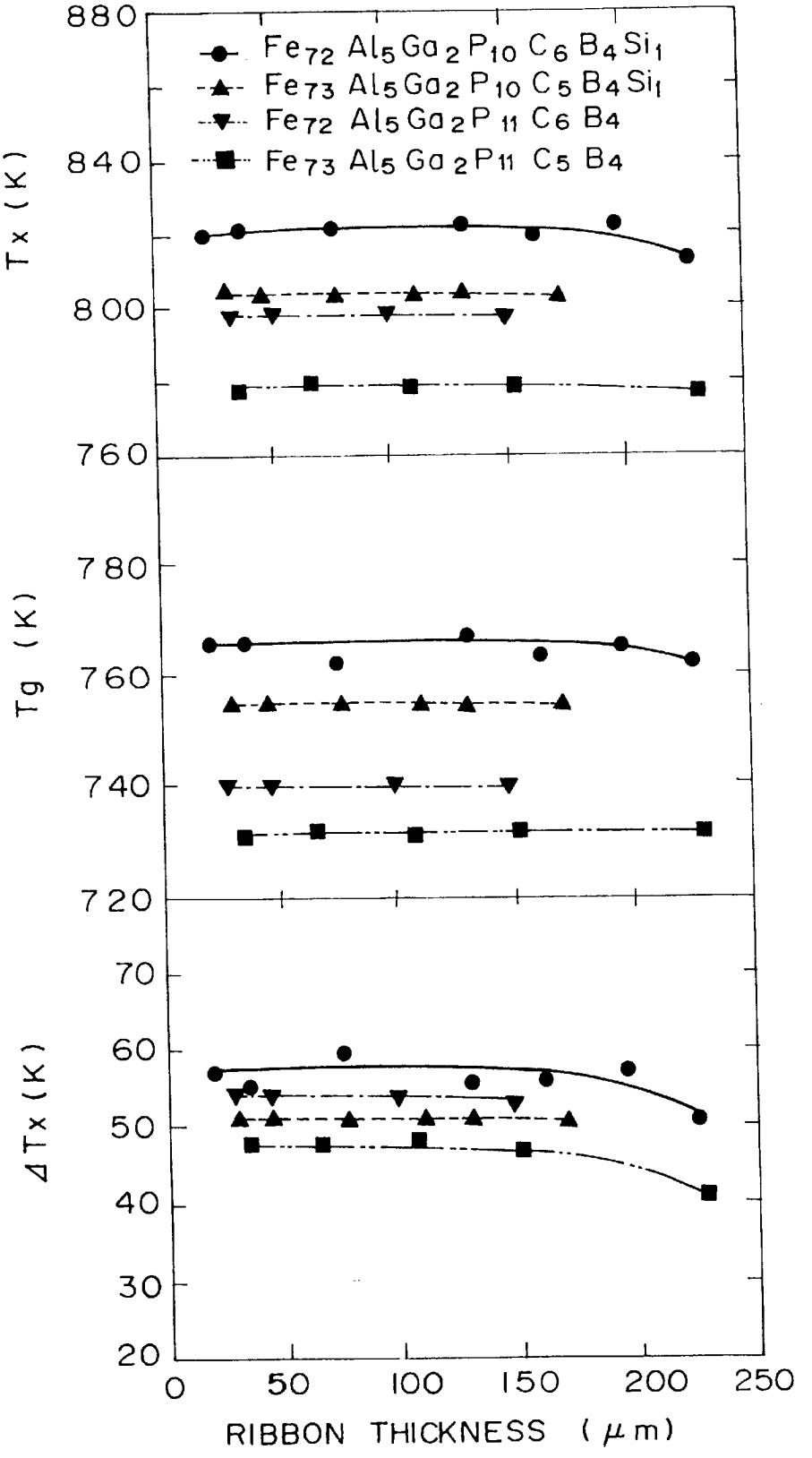
Fe72 Al5 Ga2 P10 C6 B4 Si1
Fe73 Al5 Ga2 P10 C5 B4 Si1
Fe72 Al5 Ga2 P11 C6 B4
Fe73 Al5 Ga2 P11 C5 B4
Tx (K)
Tg (K)
ΔTx (K)
880
840
800
760
780
760
740
720
70
60
50
40
30
20
0
50
100
150
200
250
RIBBON THICKNESS (μm)

FIG. 22

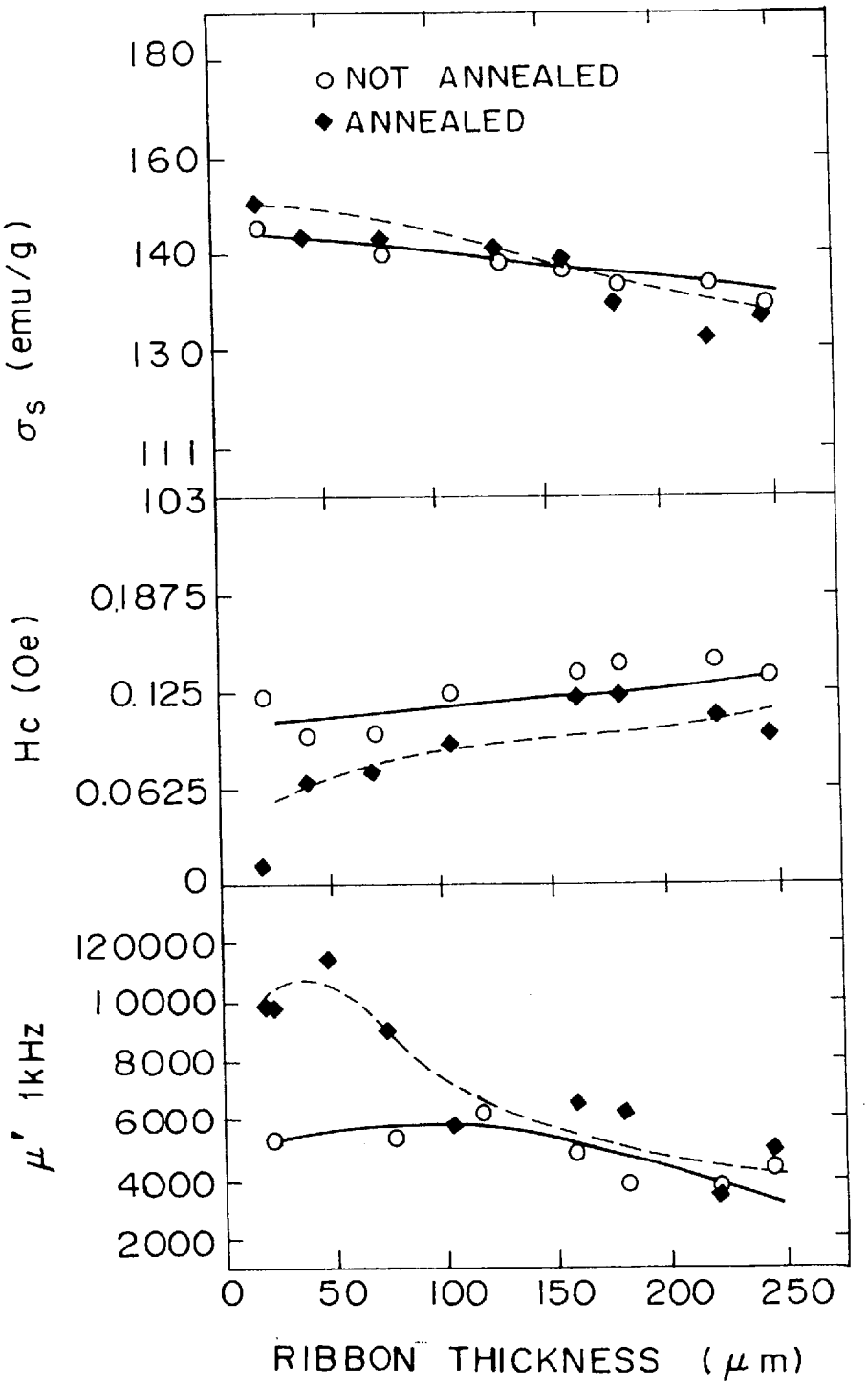
180
160
140
130
111
103
σs (emu/g)
o NOT ANNEALED
◆ ANNEALED
0.1875
0.125
0.0625
0
Hc (Oe)
120000
10000
8000
6000
4000
2000
μ' 1kHz
0
50
100
150
200
250
RIBBON THICKNESS (μm)

FIG. 23

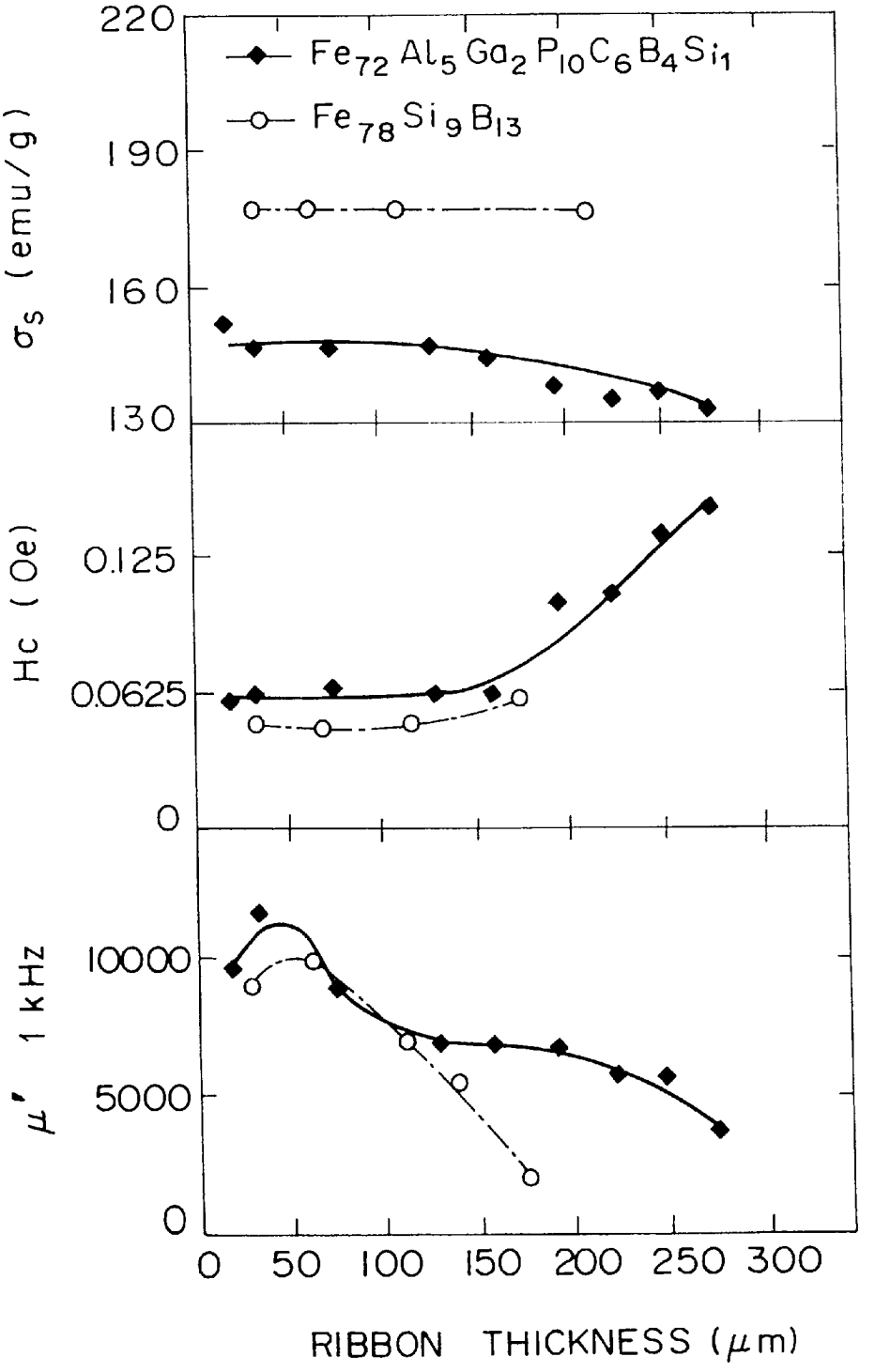
220
190
160
130
σ_s (emu/g)
$Fe_{72}Al_5Ga_2P_{10}C_6B_4Si_1$
$Fe_{78}Si_9B_{13}$
0.125
0.0625
0
Hc (Oe)
10000
5000
0
μ' 1 kHz
0 50 100 150 200 250 300
RIBBON THICKNESS (μm)

FIG. 24

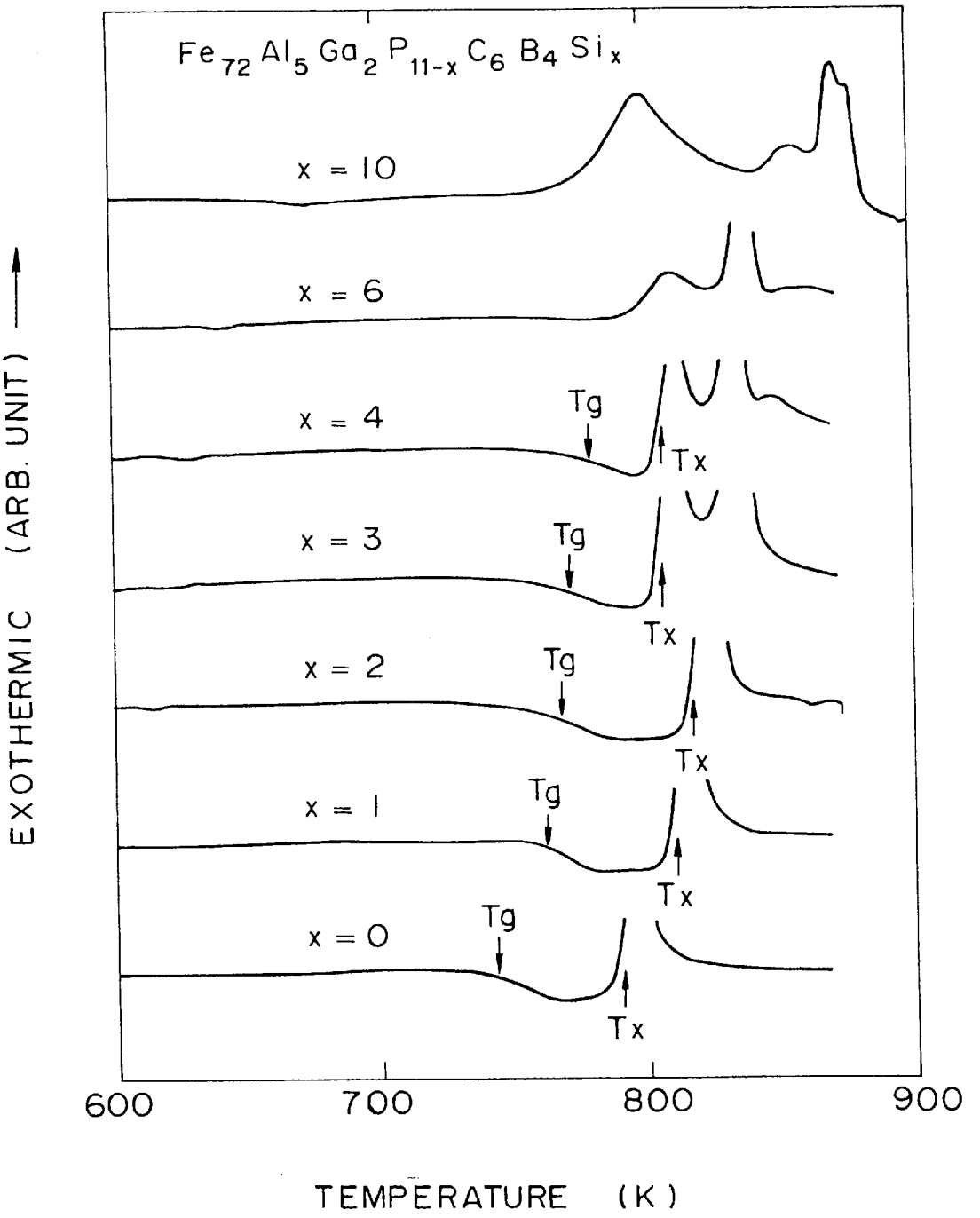
$Fe_{72}Al_5Ga_2P_{11-x}C_6B_4Si_x$
x = 10
x = 6
x = 4
x = 3
x = 2
x = 1
x = 0
Tg
Tx
EXOTHERMIC (ARB. UNIT)
600
700
800
900
TEMPERATURE (K)

FIG. 25

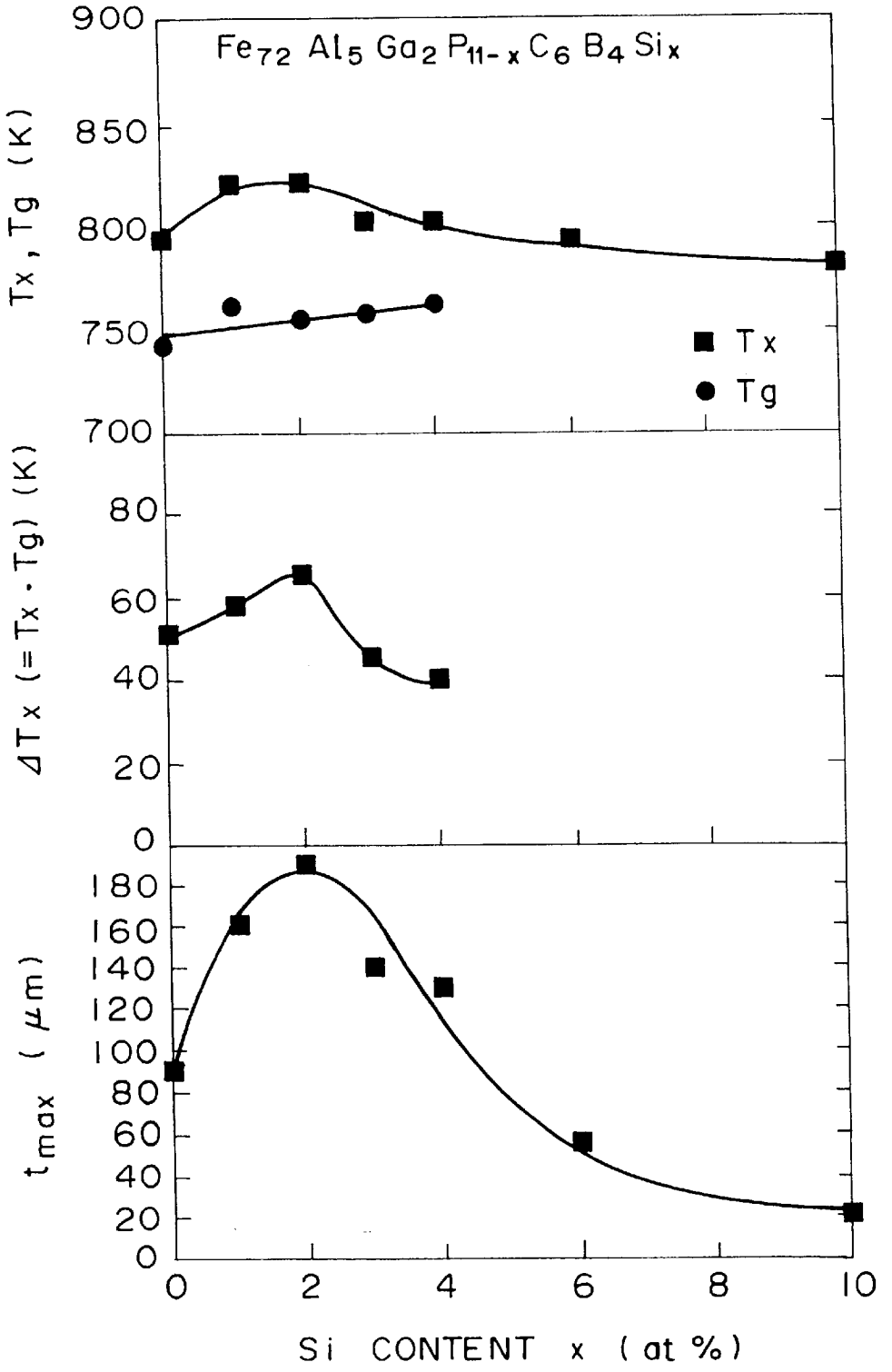
Fe72 Al5 Ga2 P11-x C6 B4 Six
Tx, Tg (K)
900
850
800
750
700
Tx
Tg
ΔTx (= Tx - Tg) (K)
80
60
40
20
0
tmax (μm)
180
160
140
120
100
80
60
40
20
0
0
2
4
6
8
10
Si CONTENT x (at %)

FIG. 26

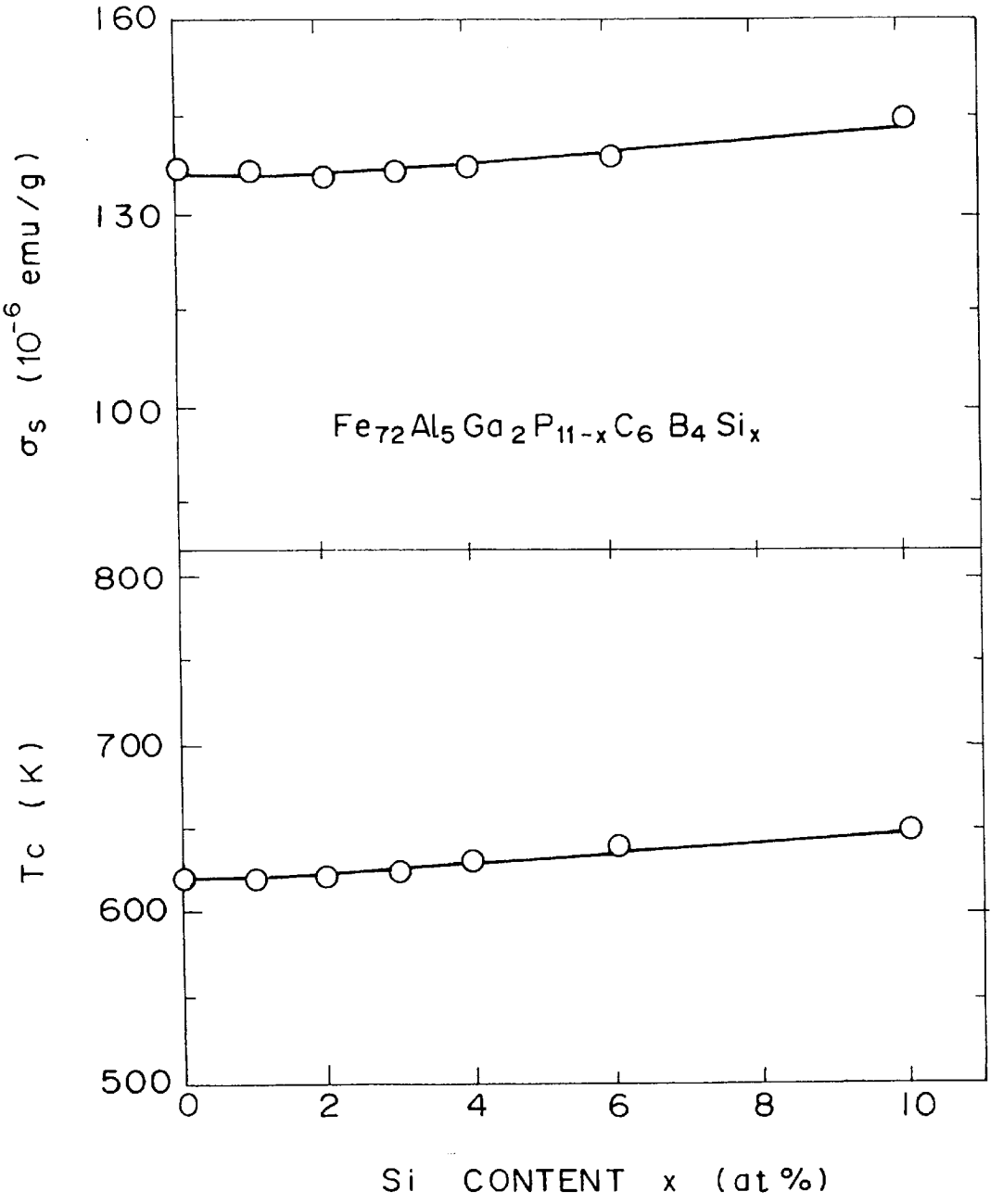
160
130
100
σ_s (10^{-6} emu/g)
$Fe_{72}Al_5Ga_2P_{11-x}C_6B_4Si_x$
800
700
600
500
Tc (K)
0
2
4
6
8
10
Si CONTENT x (at %)

FIG. 27

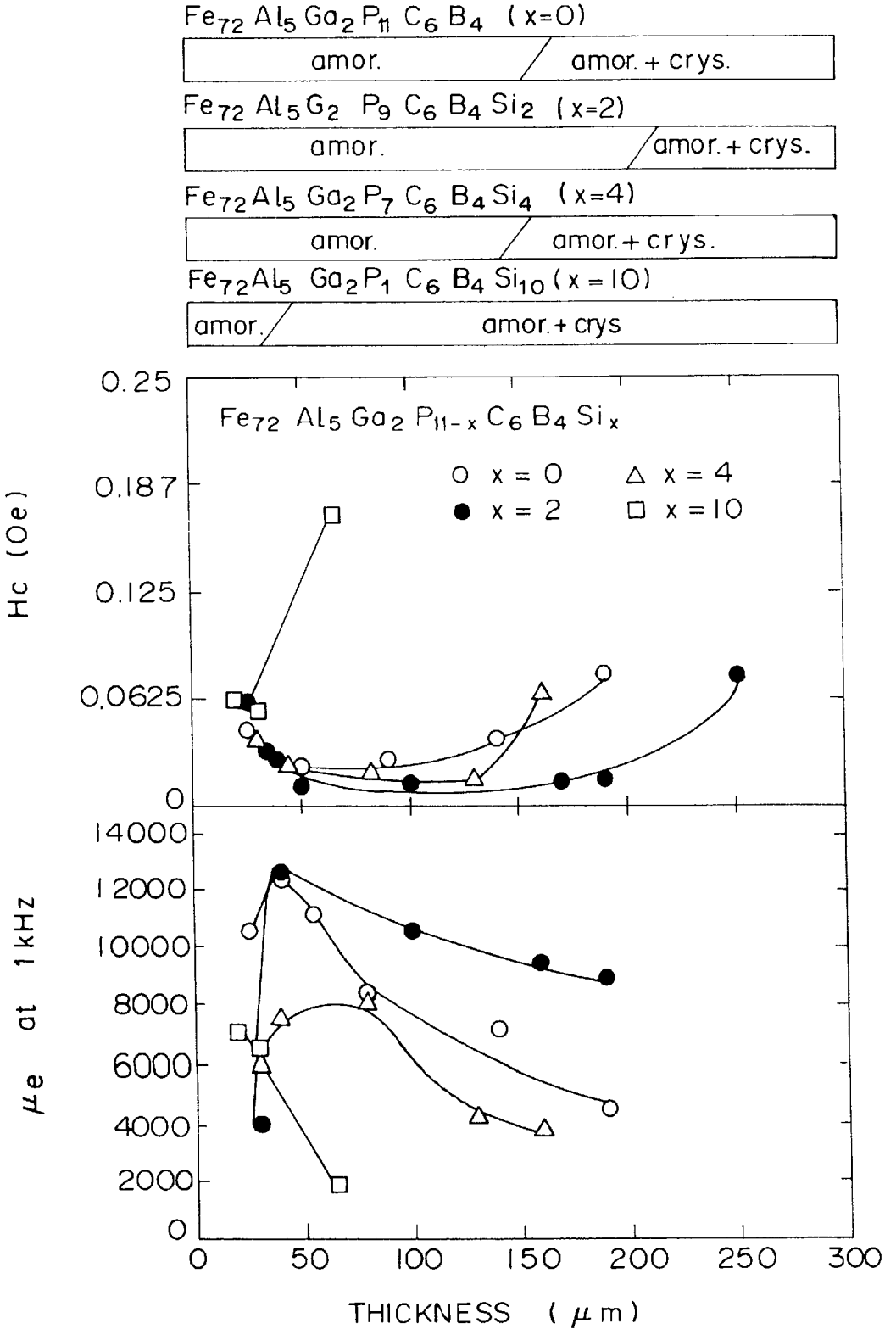
Fe72 Al5 Ga2 P11 C6 B4 (x=0)
amor.
amor. + crys.
Fe72 Al5 G2 P9 C6 B4 Si2 (x=2)
amor.
amor. + crys.
Fe72 Al5 Ga2 P7 C6 B4 Si4 (x=4)
amor.
amor. + crys.
Fe72 Al5 Ga2 P1 C6 B4 Si10 (x=10)
amor.
amor. + crys
Fe72 Al5 Ga2 P11-x C6 B4 Six
○ x = 0
● x = 2
△ x = 4
□ x = 10
Hc (Oe)
0.25
0.187
0.125
0.0625
0
μe at 1kHz
14000
12000
10000
8000
6000
4000
2000
0
0
50
100
150
200
250
300
THICKNESS (μm)

FE BASED SOFT MAGNETIC GLASSY ALLOY

BACKGROUND OF THE INVENTION

1. Field of the Invention

The present invention relates to a Fe based glassy alloy having a larger thickness as compared to prior art amorphous alloy ribbons, and exhibiting excellent magnetic characteristics and high resistivity.

2. Description of the Related Art

It has been known that some multi-element amorphous alloys have wide supercooling temperature ranges before crystallization and form glassy alloys. Also, it has been known that such glassy alloys can be formed as bulk alloys having significantly larger thicknesses than amorphous alloy ribbons formed by prior art liquid quenching processes.

Examples of prior art glassy alloys include Ln-Al-TM alloys, Mg-Ln-Tm alloys, Zr-Al-TM alloys, Hf-Al-TM alloys and Ti-Zr-Be-TM alloys, wherein Ln indicates a rare earth element and TM indicates a transition metal element. However, these glassy alloys do not exhibit magnetic characteristics at room temperature, and thus, they cannot be used as magnetic materials in industrial fields. Accordingly, research and development on thin bulk glassy alloys exhibiting magnetic characteristics at room temperature have been carried out.

In glassy alloys of various compositions capable of a supercooled liquid state, the temperature difference between the crystallization temperature (T_x) and the glass transition temperature (T_g), i.e., (T_x–T_g) is generally too low to form a practically useful glassy alloy. Thus, an alloy having a wide supercooled temperature range and a capability of forming a glassy alloy by supercooling has attracted attention in metallurgic fields, because such an alloy can overcome the thickness restrictions of known amorphous alloys. Accordingly, development of a glassy alloy exhibiting ferromagnetic characteristics at room temperature has been eagerly awaited.

SUMMARY OF THE INVENTION

It is an object of the present invention to provide a Fe based glassy alloy, which exhibits soft magnetic characteristics at room temperature, has a larger thickness than an amorphous alloy prepared by a conventional supercooling process, can be formed in bulk, and has a high resistivity.

In accordance with the present invention, a Fe based soft magnetic glassy alloy is characterized in that a temperature difference ΔT_x of a supercooled liquid of said glassy alloy expressed by the equation $\Delta T_x = T_x - T_g$, wherein T_x represents crystallization temperature and T_g represents glass transition temperature, is not less than 35° C., and a resistivity is not less than 1.5 $\mu\Omega$m.

The Fe based soft magnetic glassy alloy may contain a metallic element other than Fe and a metalloid element.

The metalloid element preferably comprises at least one element selected from the group consisting of P, C, B and Ge.

The metalloid element may comprise at least one element selected from the group consisting of P, C, B, Ge and Si.

The metallic element other than Fe preferably comprises at least one metallic element belonging to Groups IIIB and IVB of the Periodic Table.

The metallic element other than Fe preferably comprises at least one element selected from the group consisting of Al, Ga, In and Sn.

In one embodiment, the Fe based soft magnetic glassy alloy comprises: 1 to 10 atomic percent of Al, 0.5 to 4 atomic percent of Ga, 9 to 15 atomic percent of P, 5 to 7 atomic percent of C, 2 to 10 atomic percent of B, and the balance being Fe.

IN an alternative embodiment the Fe based soft magnetic glassy alloy comprises: 1 to 10 atomic percent of Al, 0.5 to 4 atomic percent of Ga, 9 to 15 atomic percent of P, 5 to 7 atomic percent of C, 2 to 10 atomic percent of B, 0 to 15 atomic percent of Si, and the balance being Fe.

In another alternative embodiment, the Fe based soft magnetic glassy alloy further comprises 0 to 4 atomic percent of Ge.

In yet another alternative embodiment, the Fe based soft magnetic glassy alloy further comprise not more than 7 atomic percent of at least one element selected from the group consisting of Nb, Mo, Hf, Ta, W, Zr and Cr.

The Fe based soft magnetic glassy alloy is a ribbon having a thickness of not less than 20 μm.

The Fe based soft magnetic glassy alloy is more preferably a ribbon having a thickness between 20 μm and 200 μm.

The Fe based soft magnetic glassy alloy is more preferably a ribbon having a thickness between 20 μm and 250 μm.

The Fe based soft magnetic glassy alloy has a halo X-ray diffraction pattern.

The Fe based soft magnetic glassy alloy may be annealed at a temperature between 300° C. and 500° C.

In the Fe based soft magnetic glassy alloy in accordance with the present invention, since a temperature difference ΔT_x of the supercooled liquid is not less than 35° C. and the glassy alloy has a resistivity of not less than 1.5 $\mu\Omega$m, a bulk glassy alloy, which overcomes restriction on thickness inherent in conventional amorphous alloy ribbons and exhibits soft magnetic characteristics at room temperature, can be obtained.

The Fe based soft magnetic glassy alloy in accordance with the present invention has a thickness of not less than 20 μm, particularly between 20 and 200 Δm, and more particularly between 20 and 250 μm when containing Si, has a resistivity of not less than 1.5 $\mu\Omega$m, and exhibits soft magnetic characteristics at room temperature. In detail, the bulk Fe based soft magnetic glassy alloy has high saturation magnetization, low coercive force, and high permeability.

BRIEF DESCRIPTION OF THE DRAWINGS

FIG. **1** is a graph illustrating X-ray diffraction patterns of samples having various thicknesses between 35 μm and 229 μm;

FIG. **2** includes DSC thermograms of samples having various thicknesses between 35 μm and 229 $\mu\Omega$m;

FIG. **3** includes DSC thermograms of samples having various thicknesses between 151 μm and 229 μm;

FIG. **4** is a graph illustrating change in crystallization temperature Tx, glass transition temperature Tg and ΔTx at various thicknesses;

FIG. **5** is a graph illustrating change in saturation magnetization, coercive force and permeability at various thicknesses;

FIG. **6** is a graph based on data partially extracted from FIG. **5**;

FIG. **7** is a graph illustrating X-ray diffraction patterns of a sample having a thickness of 229 μm before and after annealing;

FIG. **8** is a graph illustrating changes at various thicknesses in saturation magnetization, coercive force and permeability of samples annealed at different temperatures;

FIG. **9** is a graph based on data partially extracted from FIG. **8**;

FIG. **10** is a graph illustrating changes at various thicknesses in saturation magnetization, coercive force and permeability of samples having different compositions;

FIG. **11** is a graph illustrating correlation between maximum distortion and thickness of samples having different compositions;

FIG. **12** is a graph illustrating the dependence of permeability on thickness of a conventional Fe based amorphous material and a glassy alloys having a composition in accordance with the present invention;

FIG. **13** is a graph illustrating the dependence of resistivity on thickness of a conventional Fe based amorphous material and a glassy alloy having a composition in accordance with the present invention;

FIG. **14** is a graph including X-ray diffraction patterns of samples containing 71 to 76 atomic percent of Fe;

FIG. **15** includes graphs illustrating the dependence of crystallization temperature T_x, glass transition temperature T_g, ΔT_x and t_{max} on Fe content;

FIG. **16** includes graphs illustrating the dependence of saturation magnetization, coercive force, permeability and magnetostriction on Fe content;

FIG. **17** includes DSC thermograms of samples having compositions of $Fe_{70+x}Al_5Ga_2(P_{55}C_{25}B_{20})_{23-x}$;

FIG. **18** is a graph illustrating X-ray diffraction patterns of samples containing Si and having various thicknesses between 20 μm and 250 μm;

FIG. **19** is a graph illustrating X-ray diffraction patterns of a sample containing Si and having a thickness of 470 μm;

FIG. **20** include DSC thermograms of Si-containing samples;

FIG. **21** includes graphs illustrating the dependence of crystallization temperature T_x, glass transition temperature T_g, and ΔT_x on thickness;

FIG. **22** includes graphs illustrating the dependence of saturation magnetization, coercive force and permeability on thickness of a Si-containing sample before and after annealing;

FIG. **23** is a graph comparing the dependence of saturation magnetization, coercive force and permeability on thickness for a comparative sample and a sample formed in accordance with the present invention;

FIG. **24** includes DSC thermograms of samples having compositions of $Fe_{72}Al_5Ga_2P_{11-x}C_6B_4Si_x$;

FIG. **25** includes graphs illustrating T_x, ΔT_x and t_{max} of samples expressed by $Fe_{72}Al_5Ga_2P_{11-x}C_6B_4Si_x$and having different Si contents;

FIG. **26** includes graphs illustrating saturation magnetization and Curie points of samples expressed by $Fe_{72}Al_5Ga_2P_{11-x}C_6B_4Si_x$ and having different Si contents; and

FIG. **27** includes graphs illustrating the dependence of microstructure, coercive force and permeability on thickness of samples expressed by $Fe_{72}Al_5Ga_2P_{11-x}C_6B_4Si_x$ and having different Si contents.

DESCRIPTION OF THE PREFERRED EMBODIMENTS

The present invention will now be described with reference to the drawings.

Among Fe alloys, it has been known that Fe-P-C alloys, Fe-P-B alloys and Fe-Ni-Si-B alloys have glass transitions. However, the temperature differences ΔT_x of the supercooled liquids of these alloys are not more than 25° C., which is extremely low for practically forming glassy alloys.

In contrast, the Fe based soft magnetic glassy alloy in accordance with the present invention has an unexpectedly large temperature difference ΔT_x of more than 35° C., or more than 40–50° C. for specific compositions. Further, the Fe based soft magnetic glassy alloy exhibits excellent soft magnetic characteristics at room temperature. Moreover, a bulk glassy alloy, which is significantly useful as compared to amorphous alloy ribbon, is obtainable from the Fe based composition.

The Fe based soft magnetic glassy alloy has a composition comprising Fe as a major component, a metallic element other than Fe and a metalloid element. The metallic element other than Fe is selected from the group consisting of Groups IIA, IIIA, IIIB, IVA, IVB, VA, VIA and VIIA elements of the Periodic Table. Among them, Groups IIIB and IVB elements are preferably used. Examples of preferred metallic elements include Al (aluminum), Ga (gallium), In (indium) and Sn (tin). The Fe based soft magnetic glassy alloy may further contain at least one metallic element selected from the group consisting of Ti (titanium), Hf (hafnium), Cu (copper), Mn (manganese), Nb (niobium), Mo (molybdenum), Cr (chromium), Ni (nickel), Co (cobalt), Ta (tantalum), W (tungsten) and Zr (zirconium). Examples of the metalloid elements include P (phosphorus), C (carbon), B (boron), Si (silicon) and Ge (germanium).

In detail, the Fe based soft magnetic glassy alloy in accordance with the present invention comprises: 1 to 10 atomic percent of Al, 0.5 to 4 atomic percent of Ga, 9 to 15 atomic percent of P, 5 to 7 atomic percent of C, 2 to 10 atomic percent of B, and the balance being Fe and incidental impurities.

Addition of Si increases the temperature difference ΔT_x of the supercooled liquid, and thus increases the critical thickness to form a single amorphous phase. As a result, a thicker glassy alloy having superior soft magnetic characteristics at room temperature can be prepared. When excessive Si is present, the supercooling liquid region (temperature difference) ΔT_x will disappear. Thus, the preferable Si content is not more than 15%.

In detail, the Fe based soft magnetic glassy alloy preferably comprises: 1 to 10 atomic percent of Al, 0.5 to 4 atomic percent of Ga, 9 to 15 atomic percent of P, 5 to 7 atomic percent of C, 2 to 10 atomic percent of B, 0 to 15 atomic percent of Si, and the balance being Fe and incidental impurities.

The Fe based soft magnetic glassy alloy may further comprise 0 to 4 atomic percent and preferably 0.5 to 4% of Ge. Also, the Fe based soft magnetic glassy alloy may comprise not more than 7% of at least one element selected from the group consisting of Nb, Mo, Cr, Hf, W and Zr, and not more than 10% of Ni and not more than 30% of Co.

In each composition set forth above, the supercooled alloy liquid has a temperature difference ΔT_x of not less than 35° C., or not less than 40–50° C. in specified compositions.

The Fe based soft magnetic glassy alloy in accordance with the present invention can be produced into a desirable shape, e.g. bulk, ribbon, wire or powder, by a casting process, a quenching process with a single roll or a twin roll, an in-rotating water melt spinning process, a solution extraction process, or a high-pressure gas spraying process. The thickness or diameter of the Fe based soft magnetic glassy alloy obtained in such a manner is at least ten times larger than that of conventional amorphous alloys.

The resulting Fe based soft magnetic glassy alloy exhibits magnetic characteristics at room temperature. The magnetic characteristics are improved by annealing. Thus, the Fe based soft magnetic glassy alloy can be used in various magnetic applications.

In the production of the Fe based soft magnetic glassy alloy in accordance with the present invention, an optimal cooling rate depends on the alloy composition, the production process and the size and shape of the product. The cooling rate generally ranges from 1 to 10^4 ° C./sec. The cooling rate is determined while confirming crystal phase formation, such as a Fe_3B, Fe_2B or Fe_3P phase. In the present invention, it is preferred that there be large differences in atomic diameter between the added elements. Such large differences increase the packing density in a liquid state. As a result, the solid/liquid interfacial energy increases and crystal nucleus formation is suppressed.

EXAMPLE

The Fe based soft magnetic glassy alloy in accordance with the present invention will be described in detail with reference to Examples.

Example 1

Fe, Al, Ga, a Fe-C alloy, a Fe-P alloy, and B were weighed based on a given formulation and melted using a high frequency induction heater in a reduced pressure Ar atmosphere. An ingot having a composition of $Fe_{73}Al_5Ga_2P_{11}C_5B_4$, wherein subscripts represent atomic percent, was prepared. The ingot was melted in a crucible and injected on a rotating single roll through an ingot nozzle in a reduced Ar atmosphere to quench the melt. A series of quenched ribbons having thicknesses of 35 to 229 μm were prepared by such a single roll process while varying the nozzle diameter, the distance or gap between the nozzle tip and the roll surface, the roll rotation frequency, the injection pressure and the atmosphere pressure as set forth in Table 1.

TABLE 1

Thickness (μm)	Nozzle diameter (mm)	Gap (mm)	Rotation frequency (r.p.m.)	Injection pressure (kgf/cm^2)	Atmosphere pressure (cmHg)
108	0.42	0.3	500	0.35	−10
151	0.42	0.3	350	0.35	−10
66	0.42	0.3	800	0.35	−10
124	0.41	0.3	400	0.30	−10
125	0.41	0.3	400	0.30	−10
35	0.42	0.3	1500	0.35	−10
180	0.42	0.3	250	0.30	−10
229	0.42	0.6	250	0.40	−10

FIG. **1** is a graph including X-ray diffraction pat terns of the samples set forth in Table 1. FIG. **1** demonstrates that each sample having a thickness between 35 and 135 μm has a halo diffraction pattern and a microstructure comprising a single amorphous phase. In contrast, each sample having a thickness of 151 μm or 180 μm has a sharp diffraction peak near 2θ=50°. The sharp diffraction peak indicates the presence of Fe_2B crystal. The sample having a thickness of 229 μm has another diffraction peak, which indicates the presence of Fe_3B crystal grains, in addition to the above-mentioned diffraction peak.

These results illustrate that a ribbon having a single amorphous phase structure can be obtained in a thickness range from 35 to 135 μm from an alloy having a composition in accordance with the present invention by a single roll process. Further, each sample having a thickness between 151 and 229 μm is also mainly composed of the amorphous phase, although a compound phase precipitates.

FIGS. **2** and **3** include DSC (differential scanning calorimetric) thermograms of the ribbons set forth in Table 1. FIGS. **2** and **3** demonstrate that each alloy has a wide supercooled liquid region below the crystallization temperature, or a large temperature difference $\Delta T_x=T_x-T_g$, and the alloy exhibits a high amorphous phase formability. Further, FIG. **3** suggests that the sample having a thickness of 229 μm also includes an amorphous phase.

FIG. **4** is a graph illustrating the dependence of T_x, T_g and ΔT_x on thickness, wherein T_x, T_g and ΔT_x values were taken from the DSC thermograms in FIGS. **2** and **3**. FIG. **4** suggests that the T_x value is approximately 506° C. and not dependent on thickness, and the T_g value is also constant, i.e, 458° C., except for the sample having a thickness of 229 μm which has a slightly higher T_g value. Thus, each sample other than the sample having a thickness of 229 μm has a constant ΔT_x of approximately 47° C.

Magnetic characteristics of each ribbon were determined after annealing at temperatures between 300° C. and 450° C. Annealing was carried out at a heating rate of 180° C./min. and a holding time of 10 minutes in vacuo using an infrared image furnace. FIG. **5** is a graph illustrating the dependence of magnetic characteristics on annealing temperature of each ribbon. Data of typical samples is extracted from FIG. **5** and shown in FIG. **6** again. FIGS. **5** and **6** demonstrate that saturation magnetization (σ_s) of each sample having a thickness of 35 to 180 μm does not change by annealing at or below 400° C., similar to the as-quenched sample (expressed as as-Q in FIGS. **5** and **6**), but it decreases by annealing at 450° C. The saturation magnetization of the sample having a thickness of 229 μm reaches a maximum by annealing at 400° C. and decreases by annealing at higher temperatures. In order to clarify this phenomenon, X-ray diffraction patterns of this sample before and after annealing at 400° C. for 10 minutes were compared.

FIG. **7** is a graph illustrating this comparison. The diffraction pattern before annealing has two peaks of almost the same intensity near 2θ=50°, which are considered to be assigned to Fe_2B and Fe_3B crystal grains, whereas the peak assigned to the Fe_2B crystal grains has a higher intensity in the sample after annealing. These results suggest that only the Fe_2B crystal grains grow by annealing at a lower temperature. Saturation magnetization deterioration by annealing at over 400° C. is probably due to Fe_3B crystal grain growth. The saturation magnetization (σ_s) of two samples each having a thickness 151 μm or 180 μm does not change by annealing at or below 400° C. and this suggests that only Fe_2B crystal grains, which are present before annealing, grow by annealing at or below 400° C., and other crystal grains also grow by annealing at a higher temperature.

The coercive force (Hc) improves and reaches a minimum by annealing at 350° C. in all samples. At an annealing temperature higher than 350° C., the coercive force increases with annealing temperature. In each sample having a thickness of 151 or 180 μm, which is supposed to include crystal grains before annealing, the coercive force is slightly higher compared to samples of a single amorphous structure. Coercive force is indeterminable for the sample having a thickness of 229 μm.

The permeability of each sample is improved by annealing and reaches a maximum after annealing at 350° C.

FIG. **8** is a graph illustrating the dependence of magnetic characteristics on the thickness of each sample after anneal-

ing at different temperatures. FIG. **9** is a graph including data of a sample before annealing and after annealing at 350° C. which was extracted from FIG. **8** in order to clarify annealing effects. FIGS. **8** and **9** demonstrate that saturation magnetization σ_s does not change before annealing in each sample having a thickness of no greater than 180 μm, whereas it deteriorates in thicker samples. The coercive force (Hc) is almost constant before annealing in each sample having a thickness of no greater than 125 μm which comprises a single amorphous structure, whereas it increases in thicker samples. The coercive force decreases by annealing at or below 400° C. The permeability (μ') at 1 kHz is almost constant before annealing in each sample having a thickness of no greater than 125 μm which comprises a single amorphous structure, whereas it decreases in thicker samples. The permeability increases by annealing at or below 400° C., such an increase does not noticeably change with thickness. The permeability greatly decreases by annealing at 450° C.

Such changes in magnetic characteristics by annealing is probably due to thermal relaxation of internal stresses present in the sample before annealing. These experimental results suggest that an optimum annealing temperature T_a is approximately 350° C. Since magnetic characteristics may deteriorate by annealing at a temperature lower than he Curie temperature T_c due to magnetic domain adhesion, the annealing temperature must be not less than 300° C. The magnetic characteristics after annealing at 450° C. (very near the crystallization temperature of 500° C.) are inferior compared to those before annealing, probably due to crystal nucleus formation (ordering of low order structure) or domain wall pinning due to the crystal nucleus formation. Thus, it is preferable that the annealing temperature be between 300 and 500° C., in other words, between 300 and the crystallization temperature, and more preferably between 300 and 450° C.

The results of saturation magnetization (σ_s) coercive force (Hc) and permeability (μ') of samples having different thicknesses are shown in Table 2 with their microstructures. The microstructure was determined by X-ray diffractometry (XRD) and amor. in the table indicates a single amorphous phase and amor.+crys. indicates a mixed amorphous and crystal phase.

TABLE 2

Thickness (μm)	σ_g (emu/g)	Hc (Oe)	μ (1kHz)	ΔT_x (°C.)	Structure (XRD)
108	146.7	0.057	8280	48.073	amor.
151	145.2	0.048	5786	46.801	amor. + crys.
66	143.7	0.047	7724	47.455	amor.
124	144.7	0.054	6750	46.887	amor.
135	144.0	0.047	6863	47.279	amor.
35	144.1	0.072	9769	47.719	amor.
180	145.0	0.089	4627	46.405	amor. + crys.
229	132.6	—	32	41.358	amor. + crys.

amor.: amorphous, crys.: crystal

FIG. **10** is a graph illustrating the dependence of saturation magnetization (σ_s) , coercive force (Hc) and permeability (μ') on thickness of a sample for comparison having a composition of $Fe_{78}Si_9B_{13}$ before and after annealing at 370° C. for 120 minutes, and a sample in accordance with the present invention having a composition of $Fe_{73}Al_5Ga_2P_{11}C_5B_4$ before and after annealing at 350° C. for 10 minutes. Both samples exhibit excellent magnetic characteristics without deterioration in a thickness range between 30 and 200 μm.

FIG. **11** is a graph illustrating maximum strain by a bending test of a sample for comparison having a composition of $Fe_{78}Si_9B_{13}$ after annealing at 370° C. for 120 minutes, and a sample having a composition of $Fe_{73}Al_5Ga_2P_{11}C_5B_4$ after annealing at 350° C. for 10 minutes. The bending test was performed as follows: A thin ribbon is intercalated between the tips of a pair of parallel rods and bent by gradually bringing the pair of rods together. The distance L between the rod tips when the thin ribbon broke was measured. The maximum strain (λ_f) is defined as t/(L-t), where t indicates thickness of the thin ribbon. FIG. **11** shows that the $Fe_{78}Si_9B_{13}$ sample for comparison drastically loses maximum strain with increasing thickness, in other words, becomes more brittle, whereas the decrease in maximum strain is suppressed, in other words, embrittlement is suppressed in the $Fe_{73}Al_5Ga_2P_{11}C_5B_4$ sample in accordance with the present invention. At a thickness larger than 60 μm, the sample in accordance with the present invention is more resistive to bending than the sample for comparison.

FIG. **12** is a graph for comparing the dependence of permeability on thickness of a conventional Fe based amorphous alloy having a composition of $Fe_{78}Si_9B_{13}$ with that of a Fe based glassy alloy having a composition of $Fe_{73}Al_5Ga_2P_{11}C_5B_4$ in accordance with the present invention. FIG. **12** shows that the permeability of the glassy alloy in accordance with the present invention is high in a thickness range of no greater than 60 μm, and is higher in a thickness range of not less than 80 μm compared with that of the conventional alloy. In order to achieve excellent soft magnetic characteristics, i.e., a permeability higher than 5,000, it is preferable that the thickness be in a range between 20 and 180 μm.

FIG. **13** is a graph illustrating the dependence of resistivity on thickness of a sample for comparison having a composition of $Fe_{78}Si_9B_3$ and a sample having a composition of $Fe_{73}Al_5Ga_2P_{11}C_5B_4$ in accordance with the present invention. The sample in accordance with the present invention exhibits a resistivity of not less than 1.5 μΩcm over a thickness range between 18 and 235 μm, and is higher than the sample for comparison. Thus, the glassy alloy in accordance with the present invention can exhibit low eddy current loss at high frequencies.

Example 2

A series of ribbon samples having different Fe contents and expressed by the stoichiometric formula $Fe_{70+x}Al_5Ga_2(P_{55}C_{25}B_{20})_{23-x}$ were prepared to evaluate microstructure and magnetic characteristics, according to the method set forth in Example 1. Each ribbon sample was adjusted to a thickness of 30 μm.

FIG. **14** includes X-ray diffraction patterns of the resulting samples. As shown in FIG. **14**, samples having Fe contents between 71 and 75 atomic percent (X=1 to 5 in the stoichiometric formula) exhibit halo patterns and thus are composed of a single amorphous phase microstructure. On the other hand, the sample containing 76 atomic percent of Fe (x=6 in the stoichiometric formula) exhibits sharp diffraction peaks (marked with ○ in the figure) probably due to bcc-Fe crystal formation.

FIG. **15** is a graph illustrating the dependence of T_x and T_g on Fe content of a series of samples expressed by the stoichiometric formula Fe_{67+x}, $Al_5Ga_2(P_{55}C_{25}B_{20})_{26-x}$, in which T_x and T_g were determined from their respective DSC thermograms (not shown in the figure). The thickness of each sample was 30 μm. FIG. **15** shows that the T_x decreases

with Fe content over a Fe content range between 67 and 75 atomic percent (x'=0 to 8 in the stoichiometric formula). T_g also decreases with Fe content. ΔT_x determined from T_x and T_g ranges from 35 to 70° C. The t_{max} value or maximum thickness, obtainable for a ribbon composed entirely of amorphous phase, has a peak at 70 atomic percent of Fe, is not less than 150 μm at 69 to 71 atomic percent of Fe, and not less than 110 μm at 67 to 75 atomic percent.

FIG. **16** is a graph illustrating magnetic characteristics of ribbon samples expressed by the stoichiometric formula Fe_{67+x}, $Al_5Ga_2(_{55}C_{25}B_{20})_{26-x}$ after annealing of a heating rate 180° C./sec., a holding temperature of 350° C., and a holding time of 30 minutes. FIG. **16** also shows magnetic characteristics (broken lines) of a conventional $Fe_{78}Si_9B_{13}$ amorphous alloy ribbon having a thickness of 25 μm after annealing at 370° C. for 120 minutes in vacuo for comparison. FIG. **16** demonstrates that the saturation magnetization (σ_s) increases with Fe content. The saturation magnetization is 150 emu/g at 71 atomic percent of Fe and is almost the same as the Fe-Si-B based sample (σ_e=183 emu/g) for comparison.

The coercive force (Hc) is almost constant up to a Fe content of 75 atomic percent of which a single amorphous phase microstructure can be achieved.

The sample has a permeability (μ') at 1 kHz of approximately 20,000 for a Fe content of 70 atomic percent, of not less than 15,000 for a Fe content of 69 to 72 atomic percent, and of not less than 11,000 for a Fe content of 69 to 76 atomic percent. Thus, the samples in accordance with the present invention exhibit superior soft magnetic characteristics than the conventional amorphous sample for comparison.

Further, the samples in accordance with the present invention exhibit superior magnetostriction for a Fe content of between 68 and 74 atomic percent than the conventional amorphous alloy and exhibits the same value for a Fe content of 75 atomic percent.

As a result, the saturation magnetization can be improved by increasing the Fe content in the Fe based soft magnetic glassy alloy in accordance with the present invention, and a glassy alloy having a composition of $Fe_{70}Al_5Ga_2P_{12.65}C_{5.75}B_{4.6}$ and having almost the same saturation magnetization as the conventional Fe-Si-B based amorphous alloy can be produced by a single roll quenching process.

FIG. **17** shows DSC thermograms of samples having a thickness of 30 μn expressed by the stoichiometric formula $Fe_{70+x}A1_5$ $(P_{55}C_{25}B_{20})_{23-x}$wherein x'1, 2, 5 or 6. DSC thermograms were obtained at a heating rate of 0.67° C./sec. FIG. **17** demonstrates that T_g and T_x increase and ΔT_x decreases with Fe content. Tg disappears at a Fe content of 76 atomic percent, and deposition of compound phase such as α-Fe and Fe_3B phases is observed. Thus, the glassy alloy in accordance with the present invention has a supercooled liquid region for a Fe content of 75 atomic percent and high amorphous phase formability.

Example 3

Advantages of a Fe based soft magnetic glassy alloy having a composition set forth in Example 1 and further containing Si will be described in this example.

An alloy ingot having a composition of $Fe_{72}Al_5Ga_2P_{10}C_6B_4Si_1$ was prepared and melted in a crucible. The melt was injected on a rotating roll through a crucible nozzle in a reduced pressure Ar atmosphere (−10 cmHg), at a nozzle diameter of 0.4 to 0.5 mm, a distance (gap) between the nozzle tip and the roll surface of 0.3 mm, a roll rotation frequency of 200 to 2,500 rpm, an injection pressure of 0.35 to 0.40 kgf/cm^2, and a roll surface of #1,000. A series of quenched ribbons each having a thickness of 20 to 250 μm were prepared by such a single roll process. The side of the ribbon in contact with the roll surface is referred to as the roll side, and its rear side is referred to as the free side.

FIG. **18** shows X-ray diffraction patterns of the free side of the resulting ribbon samples. As demonstrated in FIG. **18**, each sample having a thickness between 20 and 160 μm has a halo pattern at 2θ=40 to 60° indicating a single amorphous phase microstructure. In each sample having a thickness of not less than 170 μm, a sharp diffraction peak was observed at approximately 2θ=50°. It is considered that this peak is assigned to a Fe_3C and Fe_3B crystal phase.

The results set forth above demonstrate that ribbons having a thickness between 20 and 160 μm and a single amorphous phase microstructure can be prepared by a single roll process. In Example 1 set forth above, a single amorphous phase microstructure can be formed in a glassy alloy ribbon having a thickness of no greater than approximately 135 μm, and a peak due to crystal grain precipitation is observed from a glassy alloy ribbon having a thickness of 151 μm. Thus, addition of Si evidently increases the critical thickness in which a single amorphous phase microstructure can be formed.

FIG. **19** shows X-ray diffraction patterns of the roll and free sides of a ribbon sample (not annealed) having the same composition ($Fe_{72}Al_5Ga_2P_{10}C_6B_4Si_1$) as above and a thickness of approximately 470 μm. Although an amorphous phase can easily be formed in Si-containing alloys, both the free and roll sides are crystallized in this sample having a thickness over the critical thickness.

FIG. **20** shows DSC thermograms of ribbon samples each having a thickness between 22 and 220 μm, at a heating rate of 0.67° C./sec. FIG. **20** demonstrates that each alloy has a supercooled liquid region over a wide temperature range below the crystallization temperature or a large ΔT_x value ($=T_x-T_g$) as in Example 1. Thus, these alloys evidently have high amorphous phase formability.

FIG. **21** shows the correlation between T_x, T_g or ΔT_x and thickness of Si-free alloy samples and Si-containing alloy samples. T_x, T_g and ΔT_x were each determined from DSC thermograms of two Si-free samples, i.e., $Fe_{72}Al_5Ga_2P_{11}C_6B_4$ (▼) and $Fe_{73}Al_5Ga_2P_{11}C_5B_4$ (■), and two Si-containing samples, i.e., $Fe_{72}Al_5Ga_2P_{10}C_6B_4Si_1$ (●) and $Fe_{73}Al_5Ga_2P_{10}C_5B_4Si_1$ (▲), in which 1 atomic percent of P in the Si-free samples is replaced with Si in the Si-containing samples. FIG. **21** illustrates that none of T_x, T_g and ΔT_x significantly change with thickness. The Si-containing samples $Fe_{72}Al_5Ga_2P_{10}C_6B_4Si_1$ and $Fe_{73}Al_5Ga_2P_{10}C_5B_4Si_1$ have ΔT_x values of approximately 57° C. and 51° C., respectively, whereas the Si-free samples $Fe_{72}Al_5Ga_2P_{11}C_6B_4$ and $Fe_{73}Al_5Ga_2P_{11}C_5B_4$ have ΔT_x values of approximately 54° C. and 47° C., respectively. Therefore, addition of Si increases ΔT_x by approximately 3 to 4° C.

Magnetic characteristics of each ribbon sample having a thickness between 20 and 250 μm before annealing and after annealing were measured. FIG. **22** is a graph illustrating the dependence of magnetic characteristics on the thickness. Annealing was performed in vacuo using an infrared image furnace at a heating rate of 180° C./min., a holding temperature of 350° C. and a holding time of 30 minutes, in which the annealing conditions were the optimum conditions for the Si-free samples in Example 1.

FIG. **22** illustrates that the saturation magnetization (σ_s) before annealing is approximately 145 emu/g independent of thickness. The saturation magnetization does not substantially change by annealing at a thickness of 160 μm or less, and decreases by annealing at a thickness over than that. This is probably due to growth of crystal grains, such as Fe_3B and Fe_3C.

The coercive force (Hc) before annealing increases with thickness. The coercive force after annealing is lower than that before annealing, and ranges from 0.635 to 0.125 Oe over the entire thickness region. Such a decrease in coercive force by annealing is probably due to relaxation of internal stresses by annealing as in Example 1. As a result of comparison of FIG. **22** with FIG. **9**, the coercive force (Hc) of the Si-containing Fe based soft magnetic glassy alloy before annealing is higher than that of the Si-free glassy alloy over the entire thickness range. However, the coercive force of the Si-containing glassy alloy decreases by annealing to almost the same level as the Si-free glassy alloy.

The permeability (μ') at 1 kHz of each sample before annealing decreases with thickness. The permeability is improved by annealing and reaches almost the same level as that of the Si-free Fe based soft magnetic glassy alloy. The annealing effect decreases with thickness, similar to Example 1.

The results of saturation magnetization (σ_s), coercive force (Hc), permeability (μ') and microstructure of samples having various thicknesses are shown in Table 3. The microstructure was determined by XRD (X-ray diffractometry). In Table 3, amor. indicates an amorphous phase, and amor.+crys. indicates an amorphous and crystal mixed phase.

TABLE 3

Thickness (μm)	Hc (Oe)	σ_g (emu/g)	μ' (1kHz)	ΔT_x (°C.)	Structure (XRD)
20	0.059	147.3	9500	57	amor.
50	0.051	146.5	11300	55	amor.
72	0.049	145.0	9000	59	amor.
90	0.053	143.3	7500	57	amor.
105	0.054	142.5	7000	58	amor.
130	0.063	141.7	6000	56	amor.
160	0.063	142.5	5500	57	amor.
173	0.071	142.5	5200	54	amor. + crys.
220	0.11	137.7	4500	52	amor. + crys.
250	0.15	135.4	4000	50	amor. + crys.

amor.: amorphous, crys.: crystal

FIG. **23** is a graph illustrating the dependence of saturation magnetization (σ_s) , coercive force (Hc) and permeability (μ') on thickness of a sample for comparison having a composition of $Fe_{78}Si_9B_{13}$ and a sample in accordance with the present invention having a composition of $Fe_{72}Al_5Ga_2P_{10}C_6B_4Si_1$, which are annealed at 350° C. for 30 minutes. FIG. **23** illustrates that the Fe based glassy alloy sample of the present invention exhibits less characteristic magnetic deterioration over a thickness range between 20 and 250 μm as compared to the conventional amorphous alloy sample for comparison. In particular, the sample of the present invention exhibits superior permeability, i.e., not less than 5,000 over a thickness range between 20 and 250 μm and thus superior soft magnetic characteristics than the conventional sample.

Example 4

Changes in thermal and magnetic characteristics, when the Si content is varied in the sample used in Example 3, were studied in this example.

FIG. **24** shows DSC thermograms of samples having compositions expressed by $Fe_{72}Al_5Ga_2P_{11-x}C_6B_4Si_x$, wherein x=0, 1, 2, 3, 4, 6 and 10. In FIG. **24**, glass transition (Tg) is observed in each sample having a Si content between 0 and 4 atomic percent, suggesting the existence of a supercooled region. Thus, it is preferred that the Si content be not more than 4 atomic percent in order to achieve high amorphous phase formability.

FIG. **25** shows the dependence of T_x, ΔT_x and t_{max} on Si content. FIG. **25** demonstrates that ΔT_x and t_{max} have maximum values at a Si content of 2 atomic percent and the preferable Si content to achieve a t_{max} value of not less than 100 μm ranges from 1 to 4 atomic percent.

FIG. **26** shows the dependence of saturation magnetization (σ_s) and Curie point (T_c) on Si content. As shown in FIG. **25**, both the saturation magnetization (σ_s) and Curie point (T_c) are satisfactory levels for a Si content range of 10 atomic percent or less and slightly increase with Si content. Even for a Si content range of over 4 atomic percent without a ΔT_x value, they are at practical levels for some application fields.

FIG. **27** shows the dependence of coercive force (Hc) and permeability (μ_e) at 1 kHz on thickness of ribbon samples having compositions expressed by $Fe_{72}Al_5Ga_2P_{11-x}C_6B_4Si_x$, wherein x=0, 2, 4 and 10, as well as microstructures. As shown in FIG. **27**, the Si-free sample has a minimum Hc value at a thickness of 70 μm and a maximum μ_e value at a thickness of 50 μm and is composed of a single amorphous phase microstructure with a thickness of not more than 150 μm. In the sample containing 2 atomic percent of Si, a low Hc value of not more than 0.05 Oe and a high μe value of not less than 9,000 are maintained over a thickness range of not more than 200 μm. A single amorphous phase microstructure is also maintained over a thickness range of not more than 200 μm. On the other hand, for a thickness range of less than 50 μm, the μ_e value steeply decreases. Thus, the sample in accordance with the present invention exhibits excellent soft magnetic characteristics in a larger thickness region. Such excellent soft magnetic characteristics deteriorate by further increasing the Si content to 4–10 atomic percent, thereby narrowing the single amorphous phase region. However, the σ_s value is maintained at a practically high level in samples containing large amounts of Si, as illustrated in FIG. **25**, and thus these samples are useful in some application fields.

As set forth above, a Fe based soft magnetic glassy alloy in accordance with the present invention exhibits a temperature distance ΔT_x of a supercooled liquid of not less than 35° C. and a resistivity of not less than 1.5 $\mu\Omega$m. Thus, the bulk glassy alloy can be prepared without restriction of the thickness. Further, the glassy alloy exhibits excellent soft magnetic characteristics at room temperature.

It is preferable that the glassy alloy contains a metallic element other than Fe and a metalloid element, that the metalloid element is at least one element selected from the group consisting of P, C, B and Ge, and that the metallic element other than Fe is at least one element selected from Groups IIIB and IVB of the Periodic Table, i.e., Al, Ga, In and Sn.

A bulk Fe soft magnetic glassy alloy ribbon exhibiting a high resistivity of not less than 1.5 $\mu\Omega$m and excellent soft magnetic characteristics at room temperature is obtainable in a thickness range of not less than 20 μm, preferably from 20 to 200 μm, and, in particular, 20 to 250 μm when the alloy contains Si. The excellent soft magnetic characteristics represent high saturation magnetization, low coercive force and high permeability.

The present invention is not limited to the examples set forth above, and various changes in composition, production method, annealing condition, and shape can be made by one skilled in the art without departing from the spirit and scope of the invention.

What is claimed is:

1. An Fe based soft magnetic glassy alloy ribbon characterized in that:

a temperature difference, $\Delta T_x = T_x - T_g$, is 35° C. or more, wherein T_x represents the crystallization temperature of the glassy alloy; T_g represents the glass transition temperature of the glassy alloy; resistivity of 1.5 $\mu\Omega$m or more; a ribbon thickness in the range of 25 to 250 μm; comprising:

0 to 10 atomic percent of Al,

0.5 to 4 atomic percent of Ga,

9 to 15 atomic percent of P,

5 to 7 atomic percent of C,

2 to 10 atomic percent of B,

4 to 10 atomic percent of Si, and

Fe.

* * * * *

UNITED STATES PATENT AND TRADEMARK OFFICE

CERTIFICATE OF CORRECTION

PATENT NO. : 5,961,745
DATED : October 5, 1999
INVENTOR(S) : Akihisa Inoue et al.

It is certified that error appears in the above-identified patent and that said Letters Patent is hereby corrected as shown below:

On the Title Page

In column 1, item [22], please change "**Mar. 26, 1997**" to --**Mar. 25, 1997**--.

In column 2, line 9, under "**ABSTRACT**", please change "Tx" to --T_x--, and "Tg" to --T_g--.

Signed and Sealed this

Twenty-first Day of November, 2000

Attest:

Q. TODD DICKINSON

Attesting Officer

Director of Patents and Trademarks